Silk-based Tissue Engineered Constructs to Improve Tissue Regeneration and Vascularization with Stem Cells

A thesis

submitted by

Yuqi Wang

In partial fulfillment of the requirements

for the degree of

Master of Science

in

Biomedical Engineering

TUFTS UNIVERSITY

May 2018

Advisor: Dr. Lauren D. Black III, Dr. David L. Kaplan

Abstract

A silk-based hydrogel system was explored to evaluate the effects of substrate stiffness and cyclic stretch on human mesenchymal stem cell (hMSCs) differentiation. The hydrogel fibers were highly tunable, elastic and supported the survival and growth of encapsulated hMSCs. The hMSCs in silk hydrogel fibers at 50 kPa and 150 kPa both transferred from a multipotent stem cell state to a pre-osteoblast/adipocyte state in static culture. With cyclic stretching, osteo-differentiation was enhanced, while adipo-differentiation was suppressed. A new method to generate a tunable, anisotropic 3D porous scaffold with branching networks to enhance vascularization *in vitro* and direct anastomosis *in vivo* was also developed. Branched channels were generated in the silk-based scaffolds with proper endothelialization. Silk fibers in the scaffold aligned with a specific direction and achieved anisotropic diffusion of molecules with different sizes. These new silk-based tissue engineered constructs can integrate physical and chemical cues for desired stem cell differentiation to improve tissue regeneration.

Acknowledgements

I would like to thank my advisors, Dr. Lauren D. Black III and Dr. David L. Kaplan, for their mentorship, guidance, and support throughout my research and thesis work. I'm very grateful Lauren and David was willing to take me and taught me through how to think and plan independently in research. I would also like to thank Dr. Emmanuel (Manolis) S. Tzanakakis for his support and participation on my defense committee. I would like to extend my gratitude to past and present graduate students and post-docs in the Black Lab and Kaplan Lab: Dr. Whitney Stoppel, Dr. Kelly Sullivan, Dr. Lauren Baugh, Dr. Tozzi Lorenzo, Dr. Ying Chen, Dr. Xuan Mu, Dr. Benjamin Partlow, Breanna Duffy, Luke Perreault, Matt Watson and Sarah Bradner. Specifically, I would thank Dr. Whitney Stoppel for teaching me all the technics, helping me to make research plans, and guiding me through all the difficult issues during my studies. In particular, thank you to Adam Rayfield for doing the COMSOL simulation. I am also grateful for the support of Milva Ricci in keeping the department running.

Most importantly, thank you to my family for their loving support.

Table of Contents

List of Figures

Chapter 1 - Introduction

The work in this thesis describes projects I have done to investigate a new method for generating a silk-based engineered tissue construct to recapitulate the microstructure and mechanical properties of natural tissue. The effects of cyclic stretch and substrate stiffness on hMSCs differentiation were also evaluated in a silk-based hydrogel system to further optimize the design of silk scaffold loaded with stem cells, and thus improve the treatment of specific tissue regeneration.

Chapter 2 introduces the background information and the motivation of carrying out this project. The introduction begins with the clinical relevance of tissue regeneration and tissue engineered constructs in healing injured tissue, followed by an overview of biomaterial scaffolds used for tissue regeneration. The importance of vascularization is also elucidated. The necessity of systematically evaluating the effects of mechanical cues on stem cells, a key cell source in biomaterial scaffolds, differentiation in a 3D environment are also discussed. Finally, the advantages and wider application of silk biomaterials in tissue engineering are introduced. Motivations are provided that focus on the possibility of using silk for generating required tissue engineered constructs with integration of proper physical or biochemical cues to direct stem cell differentiation.

Chapter 3 presents an investigation on the effects of substrate stiffness and cyclic stretch on hMSCs differentiation using a silk hydrogel system. The results showed how these physical cues affect adipogenesis and osteogenesis in 3D silk hydrogel fibers. The findings proved the feasibility of using the silk hydrogel system for further studies.

Chapter 4 describes the newly-formed anisotropic silk-based 3D scaffold with built-in branching networks. In this chapter, the anisotropic structure and diffusion successfully mimicked natural tissue. The endothelialization of branching channels established the foundation of vascularization. In the future, the silk scaffold can be integrated with the physical cues determined using the developed silk hydrogel system.

Chapter 5 summarizes the results in these projects and also discusses the potential future directions for the generated silk-based engineered constructs.

Chapter 2 – Background

2.1 The Need for Tissue Regeneration

Tissue failure, caused by tumor, infection, ageing, trauma, etc., is one of the major life-threatening diseases [12-14]. While some tissues are able to regenerate by themselves after injury, many important tissues such as the heart, kidney and lungs have limited ability to fully restore their function. For example, cardiac tissue failure, which can result from myocardial infarction (MI), is one of the leading causes of death worldwide [15]. This is because adult cardiomyocytes have very limited proliferation.

Transplantation, the traditional treatment for tissue failure, has been explored to replace damaged tissues. However, there are still challenges including unwanted immune responses, spreading of diseases and fewer donors available for transplantation. For example, in 2018, only 2,663 donors are available for transplantation, but there are 114,924 people are on the waiting list for organ transplantation in America (United Network for Organ Sharing, 2018). Therefore, other strategies such as drug delivery, synthetic prosthesis and mechanical devices, are under development to improve the treatments for tissue regeneration. Unfortunately, these therapies cannot fully recapitulate the function of damaged tissue or organ in the long-term [16]. Tissue engineering aims to promote regeneration of all structures and functions of natural tissue and was initially promoted by Langer *et al*. in 1993. The goal of tissue engineering is to generate a

functional tissue engineered construct *in vitro* to replace the damaged tissue without the limitation of current treatments.

A tissue engineered construct is one of the major potential techniques for repairing damaged tissue and regenerating healthy tissue [17-19]. Porous 3D scaffolds are often generated using synthetic or natural biomaterials for cell seeding and growth in order to achieve formation of complex tissues or organs. Physical and biochemical cues including stiffness, topography, soluble factors, substrate ligands, mechanical and electrical stimulation can be applied to the cells in scaffolds in order to induce an appropriate environment for regeneration (**Figure 1**). The cell-laden engineered tissue constructs can be either cultured *in vitro* to form complex tissues for transplanting into injured areas, or directly transplanted into damaged regions to achieve tissue regeneration induced by the local environment *in vivo*.

2.2 Biomaterial Scaffold

Sponges and hydrogels are two major systems used for generating 3D scaffolds. (**Figure 1**) Hydrogel-based systems are more similar to natural tissues with higher water content and smaller pore sizes. However, compared to sponge-based systems, hydrogel-based systems are weaker in mechanical strength making it difficult to mimic harder tissues including bone, cartilage or muscle. Additionally, sponges can be created to have highly organized fiber direction and will maintain their structural integrity during and post-surgery [20, 21].

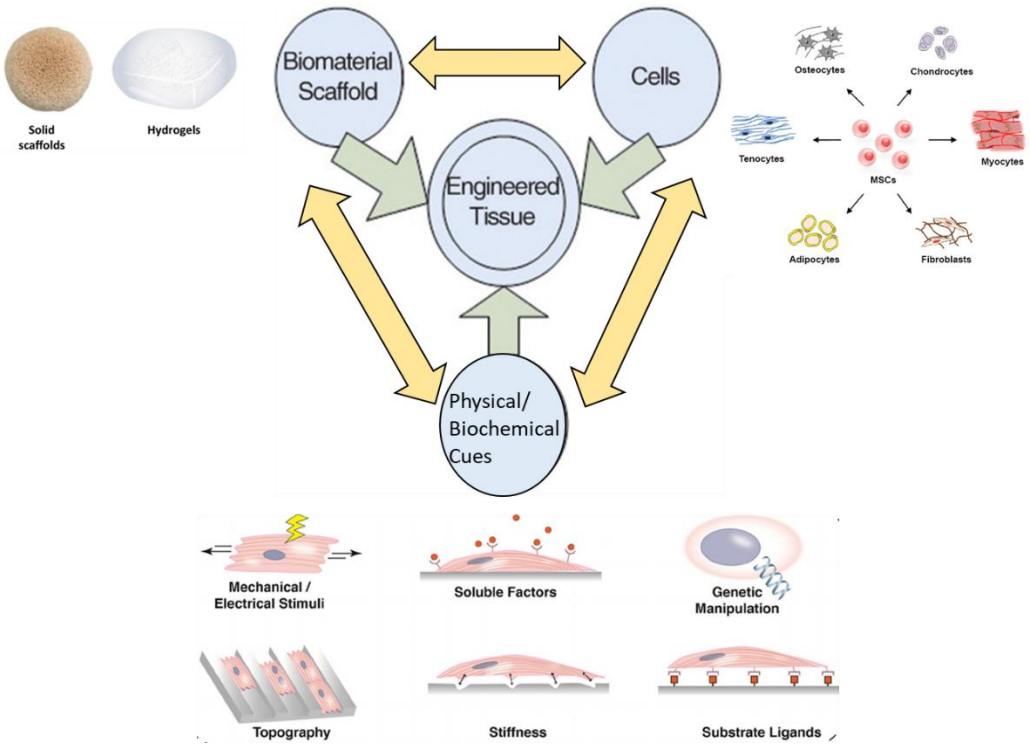

Figure 1. Tissue engineered constructs [1] are developed from cells (ex. hMSCs [8]), biomaterial scaffold (sponge-based system and hydrogel-based system[9]) and application of physical and biochemical cues such as mechanical stimuli, stiffness, topography, substrate ligands, soluble factors and genetic manipulation [11].

The biomaterials chosen for engineered tissue constructs are crucial to their success. However, it can be difficult to determine the types of biomaterials to use due to the many complexities of natural tissues. Some of these key considerations include the biomaterial's biocompatibility, biodegradability, mechanical properties, scaffold morphology and manufacturing method. Most biomaterials used now for tissue regeneration are not able to fully mimic the natural tissues and so are limited in their design. For example, currently available cardiac patches made from Dacron, PTFE or bovine pericardium are unable to mimic native mechanical strength and cannot remodel or integrate with the host tissue [22-24]. Therefore, development of a biodegradable and biocompatible engineered tissue construct that fully

recapitulates the morphology and mechanical properties of native tissue, and thus better integrates with the host tissue, is an important step in improving tissue regeneration treatments.

Synthetic polymers and natural polymers are widely used in engineered tissue constructs. Synthetic polymers including polystyrene, poly-l-lactic acid (PLLA) and polyglycolic acid (PGA) are used due to their controlled degradation rate and easy access to chemical modification. However, the biocompatibility of these synthetic polymers remains a problem especially after implantation *in vivo*. On the other hand, natural polymers such as collagen, fibronectin, or alginate showed much better biocompatibilities in supporting cell adhesion and proliferation than synthetic polymers [25, 26]. The difficulty in using natural polymers in engineered constructs comes in fabricating and modifying the polymers into a desired structure with specific properties. Furthermore, poor mechanical properties also limit the use of many natural polymers. Considering both the disadvantages and advantages in using hydrogel versus sponge-based systems or synthetic versus natural polymers, attempting to combining the two systems or two polymers together has become a potential approach to generate complex tissue engineered constructs.

To achieve clinical utility and to improve tissue regeneration, critically sized tissue engineered constructs need to be up to several millimeters thick. Because the diffusion of oxygen is limited to a distance of 100-200 μm, perfusion of blood in a thick construct is required for the cell survival and success both *in vitro* and *in vivo*. Therefore, a dense vascular network needs to be generated in the critically sized engineered constructs to deliver sufficient oxygen and nutrients. Vascular networks

can be generated in collagen, alginate and gelatin hydrogels using different techniques [27-30]. Building vessel-like structures in the tissue engineered constructs is one strategy to provide a platform for endothelialization and vessel formation. Another important strategy in forming vascular system is neoangiogenic which is based on the ability of endothelial cells to form new vessels. This can be done by adding growth factors, adhesion peptides or co-culture of several relevant types of cells (**Figure 2**). However, a major challenge using hydrogels, is not being able to achieve an anisotropic structure, which is important for achieving mechanical and electrical anisotropic in many specific tissue such as neural, muscle and heart tissue. For example, the native cardiac tissues with multilayers structure

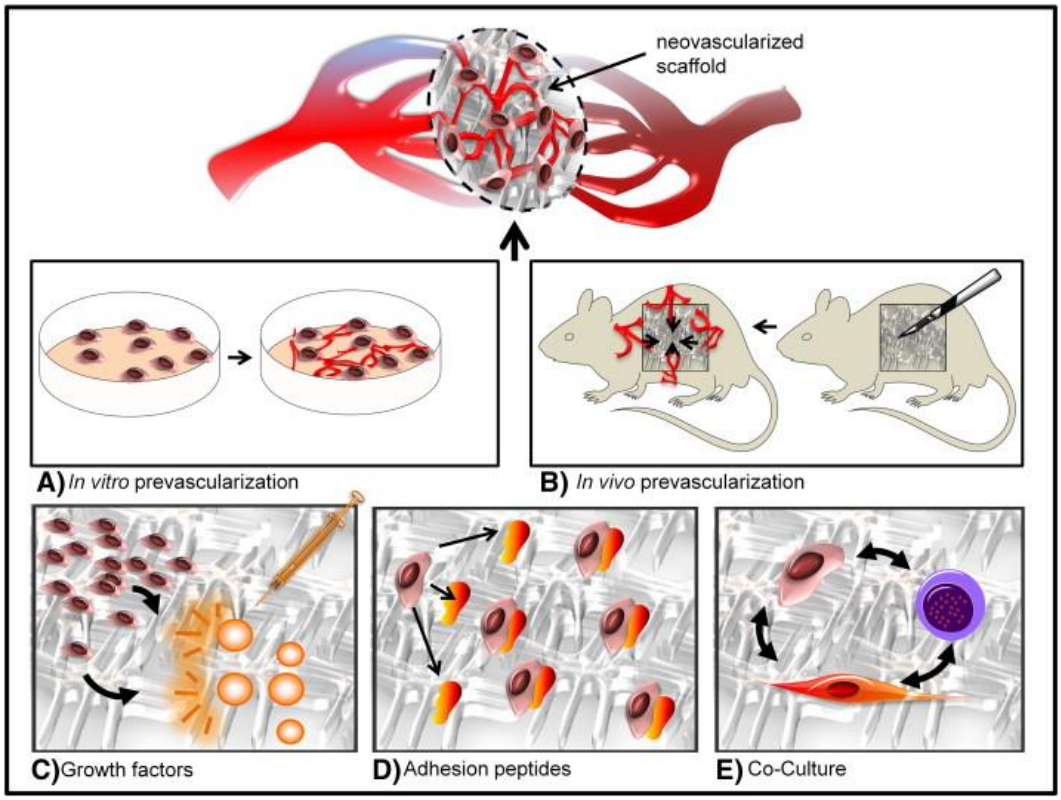

Figure 2. Five different ways to achieve vascularization through inducing neoangiogenesis [3].

containing aligned cells in each layer to achieve specific biomechanical behavior of cardiac tissue, but it is difficult to generate engineered cardiac tissues with multiple anisotropic layers in hydrogels [31].

Immediate vascular anastomosis is also necessary after implantation of these constructs [32]. Highly functional tissues including liver and heart are very sensitive to low oxygen levels and thus, immediate blood perfusion post transplantation and generation of vascularized tissue *in vivo* is necessary for cell survival. In previous studies, channels were introduced to engineered substrates to enhance vascularization and rapid anastomoses, but blood flow was still needed for several days to recover to a normal state after implantation [29]. This was probably due to the lack of proper surgical connections between host vessels and engineered vascular system. Because of these difficulties to create vascular system in tissue engineered constructs, only engineered tissue with less vessels such as bone, skin and cartilage are used now in clinics [3].

In summary, there is still a need for finding new methods to generate biocompatible and biodegradable 3D scaffolds that can be tuned to recapitulate specific tissue properties with proper vascularization for improving tissue regeneration.

2.3 Stem Cell Therapy

Cell seeding in the 3D scaffold is essential for generating functional tissues *in vitro*. Stem cells, including hESCs, iPSCs and hMSCs are well known for their ability to differentiate into several types of cells and thus reduce host rejection and immune responses. Therefore, stem cells have been considered to be a potential revolution

of clinical treatments for tissue failure [33-35]. Among all the stem cell types, hMSCs are multipotent cells with the capacity to differentiate into osteoblasts, chondrocytes, myocytes and adipocytes (**Figure 1**), and thus have been widely explored in regenerating damaged tissues including bone, cartilage, heart, liver and fat in the past few years [35]. Both MSC and MSC-conditioned medium (MSC-CM) were found to interact with inflammatory cells and induce efficient treatments of liver failure [36, 37]. A comparison between allogenic and autologous hMSCs in patients with ischemic cardiomyopathy also showed the ability to improve structural and functional recovery [38]. hMSCs have also been seeded in 3D porous scaffolds to form adipose or cartilage like tissue engineered constructs *in vitro* [39, 40].

However, unwanted differentiation and the potential to generate undesired tissue remain problems for implanted MSCs [4], especially for long-term application [7]. In a previous study, generation of calcification leading to potential bone formation was found after injection of MSCs into infarcted myocardium [4] (**Figure 3a**). More seriously, vision loss outcomes occurred in some patients one year after the injection of stem cells [7] (**Figure 3b**). These results indicate that largely unknown physical and biochemical signals in the local environment might affect the fate of transplanted stem cells *in vivo* [35]. A better understanding of the MSCs fate post-transplantation may help mitigate these risks and achieve higher efficacy of tissue regeneration. Therefore, it is important to systematically investigate the relationship between stem cell fate and environmental signals [41].

2.4 Substrate Stiffness and Stem Cell Fate

Extracellular matrix (ECM) provides structural and functional support for the stem cells as the key component of the local environment *in vivo*. Thus, to study the relationship between environmental signals and stem cell fate, several studies on the effects of physical and biochemical properties of ECM on stem cell fate have been done recently. The ECM stiffness is specific in different tissues. In mineralized bone, the ECM stiffness is over 100 kPa, while for the skeletal muscle, the stiffness is only 1 to 30 kPa. The softest tissue is fat tissue whose stiffness is only 0.5-1 kPa [2, 42] (**Figure 4a**). At the cellular level, numerous studies have

A

B

Patient Number	Preinjection Visual Acuity		Presenting Visual Acuity		Last Measured Visual Acuity	
	Right Eye	Left Eye	Right Eye	Left Eye	Right Eye	Left Eye
1	20/60	20/30	Hand motion	Hand motion	No light perception	No light perception
2	20/50	20/100	Count fingers	Count fingers	Hand motion	20/200
3	20/40	20/200	Light perception	20/200	Hand motion	Light perception

Figure 3. **a)** Von Kossa staining (left) and combined Van Gieson/ Von Kossa staining (middle and right) showed calcification and bone formation in heart after injection of MSCs [4]. **b)** The table showed clinical course of three patients receiving bilateral intravitreal injection of stem cells. All the three patients suffered significant vision decrease during the clinical treatment [7-9].

shown increased cell spreading and focal adhesion formation on stiffer substrates, such as tissue culture plastic, in a range from 1 MPa to 5 MPa [43, 44].

Experimental evidences suggest that the multipotency and differentiation of hMSCs is affected by the substrate stiffness. For example, culturing hMSCs on substrates at around 10 kPa and 30 kPa mimicking the muscle and bone tissue stiffness expressed myogenetic and osteogenic differentiation, respectively [10]. On softer hydrogels, with stiffnesses near the neural level (0.1-1 kPa), hMSCs prefer neurogenic differentiation instead (**Figure 4b**). The same trend induced by tissue specific substrate stiffness was also found in another stem cells [45, 46].

2.5 Cyclic Stretch and Stem Cell Fate

Other than substrate stiffness, transplanted stem cells also experience mechanical stimulation during body movement and normal tissue function, such as the heart beating or lung breathing. Previous studies have shown that cyclic mechanical stretch can regulate stem cell fate [47-50]. A recent study suggested that the compressed type I collagen sheet significantly increased expression of smooth muscle genes in MSCs and the combination of cyclic stretch resulted in a further enhanced smooth muscle cell phenotype [5]. Although this study failed to apply the cyclic stretch on substrates with different stiffness, it demonstrated that MSC stimulation as a result of the combination of lineage-specific matrix stiffness and mechanical loading led to differences in differentiation potential. Cyclic stretch were also found to suppress BMP-4 induced MSC adipogenesis and promote BMP-9 induced MSC osteogenesis [51, 52].

The magnitude and frequency of strain are two key parameters when applying cyclic stretch. Previous studies have indicated potential effects of different magnitudes and frequencies of strain on stem cell fate (**Figure 5**). A study of proliferation and matrix formation of MSC on Flexcell tissue train plates found that 5-15% strain at 0.5 Hz and 10% strain at 1 Hz have positive effects with upregulated cell proliferation and collagen synthesis [53]. Stem cell morphologies can also be modified by regimens of cyclic stretch [54]. Another study showed that 5% and 10% cyclic uniaxial stretch demonstrated myogenesis of MSCs, while 1% or 15% strain failed to induce myogenic lineage, indicating the importance of magnitude of strain during MSCs differentiation [55].

Therefore, studying the effects of cyclic stretch (various frequencies and magnitudes of strain) and substrate stiffness is essential for fully investigating how the local environmental signals affect stem cell fate.

2.6 Silk as a Biomaterial

Silk fibroin, a natural polymer extracted from silk cocoons, has been extensively used in tissue engineering and regenerative medicine [56]. The biocompatibility, tunable mechanical and biophysical properties, and controllable degradation rate of silk are well demonstrated in several studies [57-59]. The ability to achieve various formats including fiber, film and scaffold through different fabrication methods also enables the wide application of silk in biomedical field [60].

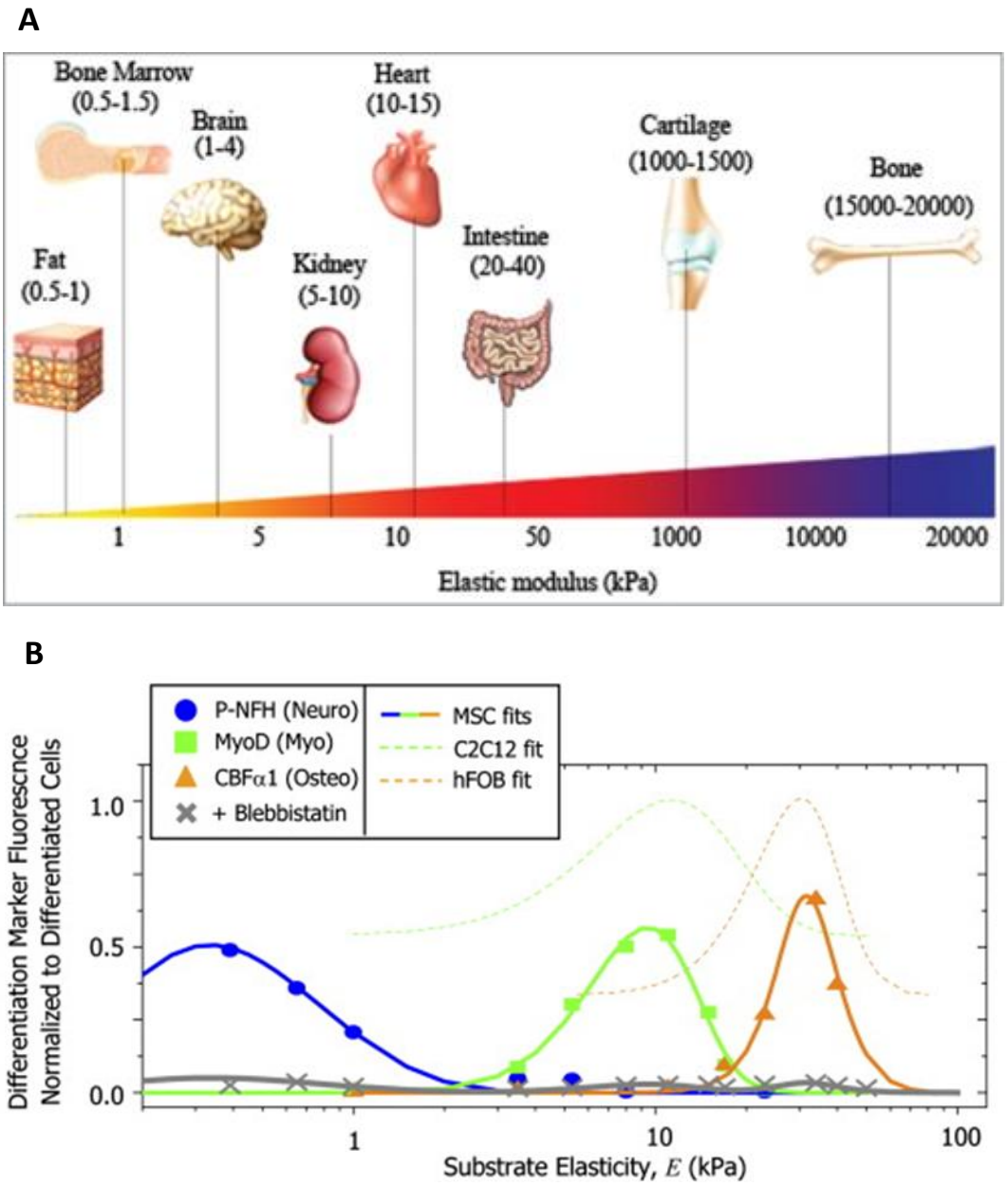

Figure 4. **a)** Elastic modulus of different tissue in human body [2]. **b)** The fluorescent intensity of differentiation markers of hMSCs on substrate with different elasticity. The results showed that neurogenesis occurs blow 1 kPa, myogenesis occurs as around 10 kPa and osteogenesis prefer substrate elasticity over 30 kPa [8, 10]

Many studies have been done previously in discovering the formation of silk sponges with tunable mechanical properties through salt leaching or freeze-drying. Previously, a biodegradable anisotropic silk patch, that incorporated cardiac ECM

(cECM), was developed using the freeze-dried silk sponges. The patch mimicked the anisotropy of heart tissue by control of the freezing direction, while addition of cECM improved cell infiltration and vascularization. Moreover, The anisotropic silk patch showed better cell adhesion and growth than the isotropic silk patch [61, 62]. A recent development of silk sponges with amorphous structure offered softer properties for engineering soft tissue *in vitro*. The kinetic controls introducing in freeze-drying processes provided the opportunity to design silk scaffolds with tunable stiffness and multiple cues [63]. Although several straight channels have been introduced into the silk sponges [64], the silk scaffolds still lack a complete endothelialized branching network with proper surgical connections to achieve surgical anastomosis *in vivo*.

Silk hydrogels can be formed through sonication [65], vortexing [66], exposure to an electrical field and chemical crosslinking [6]. Recently an enzymatically crosslinked silk hydrogel proved to be a tunable, robust and highly elastic substrate [67] (**Figure 6a**). The storage modulus varies from 200-10000 Pa with different silk concentration and boiling time (**Figure 6b**) [6]. The hydrogel remains elastic even when the strain is up to 70% with limited hysteresis (**Figure 6c**) [6]. Silk hydrogel fibers were demonstrated to be generated using this enzymatic crosslinked silk hydrogel system, with modulus from 0.5MPa to 4MPa and extensibility from 100 to 400% ultimate strain [68].

Collagen, HA and fibronectin are usually used as the substrate for studying the stem cells due to their high biocompatibility. But it is more difficult to achieve wide ranges of stiffness and strain using these hydrogels compared to silk hydrogel [69].

The limitations of modification on mechanical properties in collagen, HA, fibronectin, etc. prevent studying MSCs fate in some more extreme conditions and thus restrict further understanding of mechanical effects on MSCs fate. Although synthetic biomaterials could have a wide range of stiffness and strain, the silk hydrogel system is non-cytotoxic and supports long-term cell encapsulation and growth compared to the synthetic biomaterials [6].

Another advantage of silk as a biomaterial is that there are limited integrin binding sites on silk fibroin for cell adhesion and interaction. This provides possibilities for the addition of specific cell binding sites or specific binding of proteins. Modifications on specific substrate ligands would also contribute in guiding MSCs differentiation through specific signaling pathways [70, 71]. In conclusion, a silk hydrogel system can provide a highly tunable, elastic, long-term 3D substrate for systematically investigating effects of physical and biochemical signals on stem cell fate.

2.7 Summary

Engineered tissue constructs containing porous 3D scaffolds, cell sources and physical and biochemical cues have been recently considered to be a revolution for tissue regeneration to deal with the limitation of traditional treatments. To improve the clinical treatment of tissue regeneration, a biocompatible, biodegradable engineered tissue construct recapitulating morphology and mechanical properties of natural tissue need to be generated *in vitro*. Hydrogel-based system and sponge-

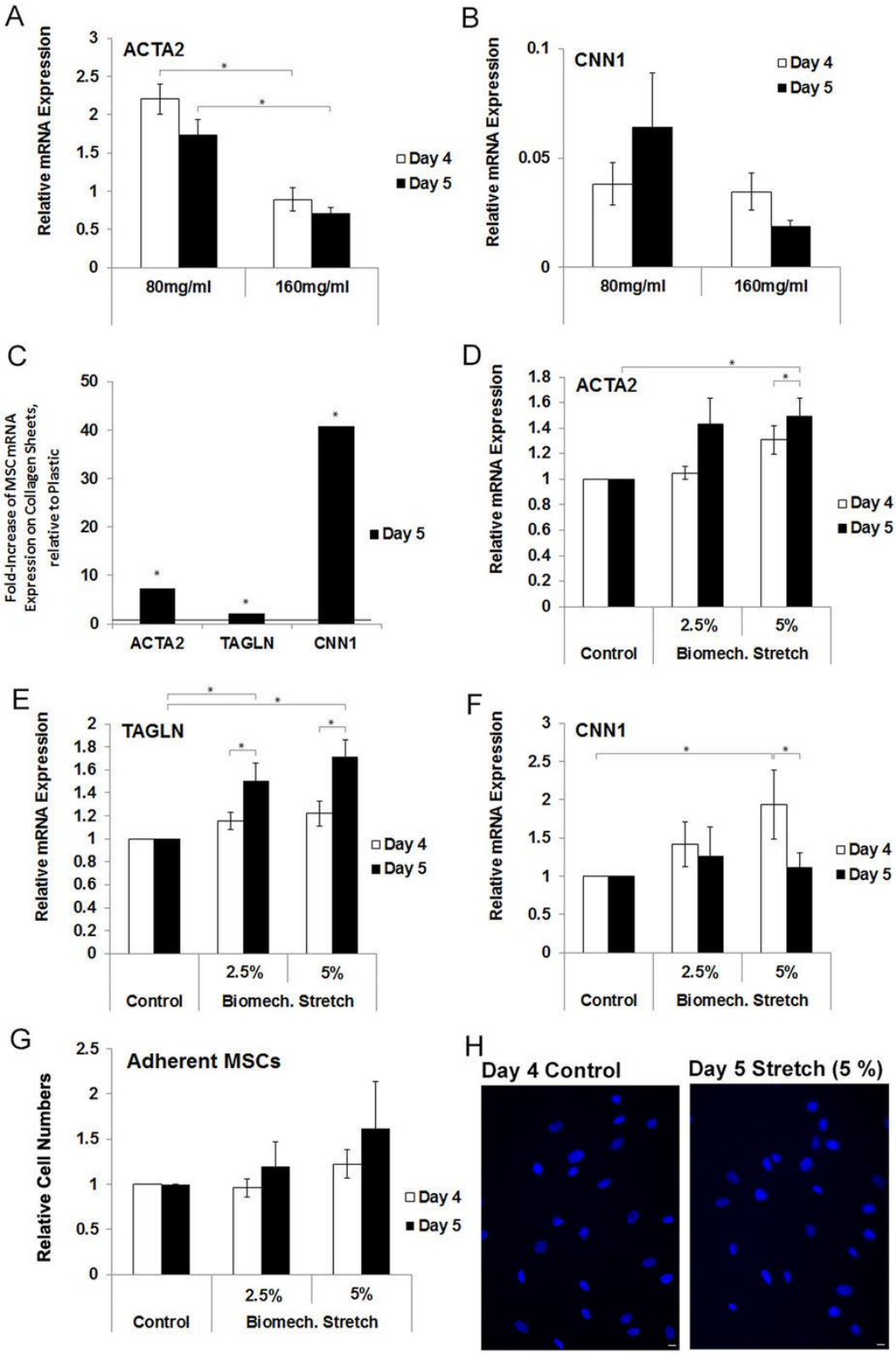

Figure 5. Gene expression, cell number of MSCs on collagen type I sheets for non-stretched control and 5% stretched MSCs [5].

based system are two major fabrication methods of porous 3D scaffolds. The hydrogel-based system is good at its similarity to natural tissue composition, and the sponge-based system has advantages in its mechanical properties and modifiable morphology.

Because both hydrogel-based system and sponge-based systems have their advantages and disadvantages, it is difficult to generate a tissue engineered construct recapitulating all functions and structure of natural tissue. Therefore, ther is a need to design new 3D scaffolds which are highly tunable to meet specific requirements of each tissue. In the 3D scaffolds, vascularization is also necessary for sufficient oxygen and nutrients delivery through immediate perfusion and efficient diffusion after transplantation.

Among all the cell sources used for tissue regeneration, stem cells are a major source given their ability to differentiate into different kinds of cells. However, the transplanted stem cells might undergo undesired differentiation and thus led to severe outcomes. In order to be able to design engineered tissue constructs with specific cues to guide desired stem cells differentiation, the effects of physical and biochemical cues on stem cell fate need to be systematically investigated *in vitro* using a highly tunable and stretchable system.

Recent studies on the application of silk fibroin in tissue engineering provided a possibility to generate new engineered tissue constructs with tunable mechanical properties, biocompatibility, controlled degradation and anisotropic structures. A newly developed silk-based hydrogel system can also be potentially used for

evaluating the effects of physical and biochemical properties on stem cell differentiation.

This project aimed to generate a new silk scaffold with endothelialized branching networks to improve the treatment of tissue regeneration. The properties of this silk scaffold will be further optimized based on the investigation of how mechanical stretch and substrate stiffness affect hMSCs differentiation. It was hypothesized that the silk-based engineered tissue constructs could successfully recapitulate the mechanical properties and anisotropic structures of natural tissue, and a silk-hydrogel system with various stiffnesses can be applied with mechanical stretch to

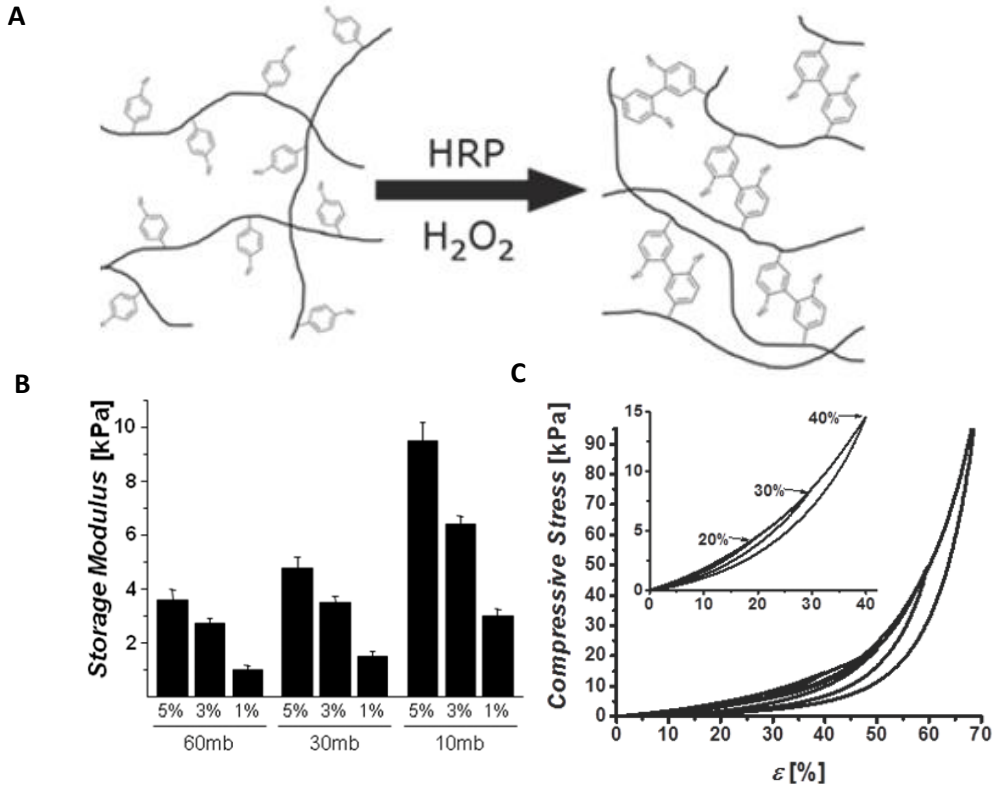

Figure 6. a) Schematic of the covalent crosslinking tyrosine residues in silk proteins. **b)** The storage modulus of silk hydrogel with different silk concentration and boiling time. **c)** stress strain curve of cyclic compression on silk hydrogel immersed in PBS. Fully recovery occurred within 40% strain [6].

study the hMSCs differentiation. The information of how specific mechanical and biochemical properties affect hMSCs differentiation could be integrated into the silk-based scaffold seeded with hMSCs in order to design the silk-based engineered tissue constructs into specific tissue regeneration such as cartilage, heart, liver, etc.

Chapter 3 – Evaluation of Effects of Substrate Stiffness and Cyclic Stretch on Stem Cell Fate in Silk Hydrogel Fibers

3.1 Introduction

Tissue failure is one of the major life-threatening diseases due to the limited ability of many important tissues such as the heart, kidney and lungs to fully restore their functions after damage or disease [12-14]. Therefore, hMSC-based therapy is one of the potential clinical treatments for healing tissue failure through tissue regeneration, which has been recently shown to improve tissue recovery due to its multipotency [72-74]. hMSCs are common stem cells used in research and clinical application to differentiate into several cell lineages such as osteogenesis, adipogenesis, neurogenesis and myogenesis [75, 76]. Direct injection of hMSCs into patients with myocardial infarction showed a 5.9% increase in left ventricular ejection fraction (LVEF) compared to the 1.6% increase in the control group [77]. However, some undesired differentiation of transplanted MSCs led to severe problems in long-term clinical trials [41]. Although several factors have been investigated to overcome this limitation [78], it remains an unsolved problem because of the lack of information regarding the effects of local environmental signals on post-transplantation hMSCs' fate [79].

It has already been well established that some chemical inductive cues and growth factors can effectively direct hMSCs differentiation into a desired lineage. However, once these cues were removed, the long-term control of hMSCs differentiation will be likely reduced, which leads to the uncontrolled differentiation occurred *in vivo*

after transplantation [80]. Thus, biomaterials with specific mechanical properties, nanotopography and composition are designed to guide hMSCs differentiation after delivery of hMSCs into injured areas [81]. ECM is a key component of the local environment *in vivo* that provides structural and functional support for the transplanted cells. The ECM stiffness is specific in different tissues with a stiffness of over 100 kPa in mineralized bone, 1 to 30 kPa for the skeletal muscle, and only 0.5-1 kPa for fat tissues [2, 42]. Different tissues usually contain specific ECM components [82, 83]. Basement membranes are full of laminins and type IV collagen, while most of the soft connective tissue contains type I and III collagen [84]. Thus, to optimize the design of biomaterials, a variety of studies have done to explore the effects of different substrate stiffness, surface roughness or incorporated proteins, which are all essential for guiding hMSCs differentiation. A study on polyacrylamide (PAAM) gel for 1 week showed that the hMSCs on stiffness over 30 kPa preferred osteogenesis while stiffness around 10 kPa led to myogenesis [10].

Moreover, transplanted hMSCs are also exposed to different kinds of mechanical stimuli including heart beating, gravity, breath, etc. Research on hMSCs differentiation under mechanical stimulation indicated that cyclic stretch inhibits adipogenesis of hMSCs through TGFβ1/Smad2 signaling pathway [85]. Increases in BMP-9 induced osteogenesis was also found in hMSCs after 12 h 1 Hz cyclic stretch [52]. Therefore, effects of substrate stiffness and cyclic stretch on hMSCs' fate are worth evaluating in order to fabricate efficient biomaterials for directing hMSCs' differentiation post-transplantation.

Previous studies used collagen, hyaluronic acid (HA), fibronectin, etc. to investigate the effects of substrate stiffness, mechanical stimulations or biochemical signals in ECM on stem cell fate. Although they have good biocompatibility, disadvantages exist for each of these substrate materials including fast degradation, difficulties for modification and narrow ranges of stiffness and strain. Because collagen, HA and fibronectin are ECM proteins, these substrates make it hard to separate the effects of pure mechanical and biochemical signals. Silk fibroin, a natural polymer extracted from silk cocoons, has been extensively used in tissue engineering and regenerative medicine [56]. The biocompatibility, tunable mechanical and biophysical properties, and controllable degradation rate of silk are well demonstrated in several studies [57-59]. A new way to form highly elastic silk hydrogel with tunable properties through horseradish peroxidase (HRP) and hydrogen peroxidase (H_2O_2) induced covalent crosslinking tyrosine residues in silk proteins was found by Parlow *et al*. [67]. The hydrogel, which remains elastic even when the strain is up to 70%, provides the opportunity to investigate long-term hMSCs' fate under changes of mechanical properties and application of cyclic stretch.

The goal of this project is to generate and evaluate the ability of a highly tunable, elastic, long-term silk hydrogel system to fully investigate the effects of substrate stiffness, cyclic stretch and ECM proteins on hMSCs' fate, and thus optimizing the design of silk scaffolds to direct differentiation of loaded hMSCs.

3.2 Methods

3.2.1 Silk Solution Preparation

Silk fibroin was extracted from *Bombyx mori* silk worm cocoons according to previously published methods [60]. 5 g Cocoons were cut into pieces and boiled in a glass beaker of 2 L Na_2CO_3 solution (0.02 M) for 60 minutes. The degummed fibers were rinsed with distilled water to remove residual Na_2CO_3 solution and air dried overnight in a chemical hood. The dried fibers were solubilized in LiBr (9.3 M, dried fibers: LiBr solution was 1 g: 4 mL) in a 60°C oven for four hours. The solubilized silk solution (15 mL to 20 mL) was dialyzed in 2L distilled water with a regenerated cellulose membrane (3,500 molecular weight cut off, Slide-A-Lyzer, Pierce, Rockford, IL). The water was changed 1 and 4 hours after starting of dialysis, followed with 4 more times of water changing in 48 hours when the LiBr was fully removed calculated by the conductivity of the dialysis water (< 5 μS cm^{-1}). The solubilized silk fibroin solution was removed from the dialysis cassettes and centrifuged for 20 mins, 3 times at 4°C to remove insoluble particulates and stored in a 4°C fridge. Silk concentration was determined by air drying 500 μL of the silk solution in a weight boat overnight at 60°C and calculating the remaining weight. The final silk solution yielded 6% to 8% (w/v).

3.2.2 Silk Hydrogel Fibers Generation

Silk solution, HRP, 10X DMEM (Sigma Aldrich, St. Louis, MO) and hMSCs were first mixed together to reach a final composition of 5% and 3% silk solution, 10 U HRP, 1X DMEM and 1×10^6 cells/mL. 1% H_2O_2, which was made through dilution of 30% H_2O_2 (Sigma Aldrich, St. Louis, MO), was added later to reach a final

concentration at 0.003%, 0.005% or 0.01% to trigger the crosslinking process. The mixed solution was drawn into a 3 mL syringe with a blunt 20-gauge needle immediately after H_2O_2 was added and left for 5-20 mins until the crosslinking process was close to the steady state. The hydrogel was then pressed out to form the fibers into the growth media (supplemented with 10% fetal bovine serum and 1% antibiotic/antimycotic) (Life Technologies, Grand Island, NY). The silk hydrogel fibers were cultured at 37 °C, 5% CO_2/95% air, and 95% relative humidity for 14 days. (**Figure 7**)

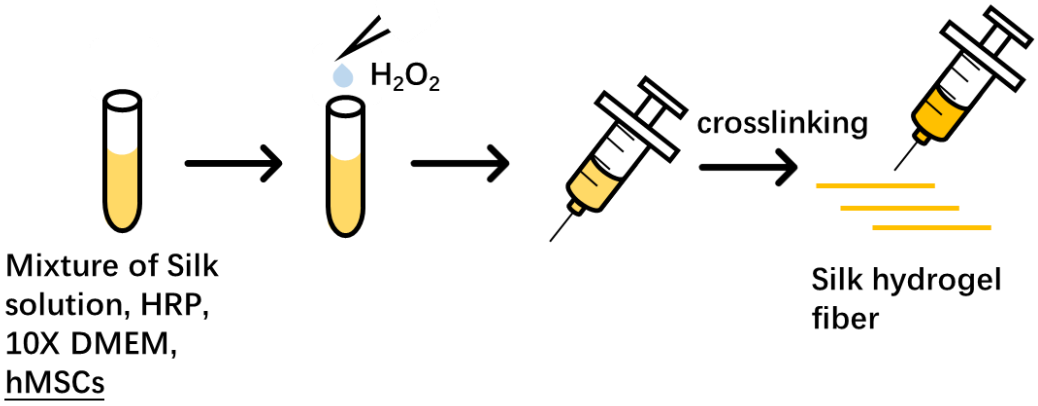

Figure 7. Schematic of silk hydrogel fiber making.

3.2.3 Stiffness Measurement

A TA Instruments RSA3 Dynamic Mechanical Analysis (DMA, TA Instruments, New Castle, DE) was used to test the stiffness of silk hydrogel fibers made with different silk concentrations at 3% and 5% on day 1 and 7 and 14 (**Figure 8a**). 60min boiled silk solution was used and three different H_2O_2 concentrations at 0.003%, 0.005% and 0.01% were tested. Samples were subjected to 4 tensile cycles to 20% strain to eliminate artifacts in a Phosphate Buffered Saline (PBS) bath. The fifth and sixth cycles were used to calculate tensile modulus which are quantified

as the tangent of the stress-strain curves at 10% strains. All fibers were stretched at a constant rate of 0.025 mm/s.

3.2.4 Cell Culture and Encapsulation

The Flex cell plate (Bio Excellence International Tech Co.,Ltd) was used for applying cyclic stretch on silk hydrogel fibers. The two ends of silk hydrogel fibers encapsulating 1×10^6 cells/mL were glued on the tissue train plates (Bio Excellence International Tech Co.,Ltd) using the silk hydrogel with same compositions without cells. Cyclic stretch at 10% strain and 1Hz frequency were applied to the silk hydrogel fibers (3% and 5% silk concentration, 0.005% H_2O_2 concentration) continuously for 24 hours using flex cell plate in the growth media (supplemented with 10% fetal bovine serum and 1% antibiotic/antimycotic) (Life Technologies, Grand Island, NY).

3.2.5 Cell Viability and Metabolic Evaluation

Silk hydrogel fibers encapsulating 1×10^6 hMSCs/mL at 3% silk concentration and 0.005% H_2O_2 concentration were made as described above in the growth media, and cultured at 37 °C, 5% CO_2/95% air, and 95% relative humidity for 21 days. 50 μL of 1×10^6 hMSCs/mL was loaded into each well in a 24 well tissue culture plate at the same culture condition.

The relative metabolic activity of the hMSCs in silk hydrogel fibers after 1, 7 and 21 days culture was determined by AlamarBlue assay (Life Technologies, Grand Island, NY) according to the manufacturer's directions. The silk hydrogel fibers were rinsed with Phosphate Buffered Saline (PBS) and incubated in DMEM

medium with 10% AlamarBlue reagent for 4 h at 37 °C, 5% CO_2/95% air, and 95% relative humidity. After incubation, 100 µL aliquots were loaded into a black 96 well plate with clear bottom. A microplate reader (Synergy™ H1, BioTek) was used to quantify the fluorescence intensity. The excitation wavelength was 550 nm and the emission wavelength was 590 nm. hMSCs seeded in 24 well tissue culture plates were used as positive control groups, while silk hydrogels fibers without hMSCs were used as negative controls.

The viability of the hMSCs in silk hydrogel fibers after 1, 14 and 21 days culture was determined by Live/Dead assay. Briefly, the silk hydrogel fibers with hMSCs were incubated with 2 µM calcein AM and 4µM ethidium homodimer-1 (EthD-1) (Thermo Fisher Scientific, Waltham, Massachusetts, USA) at room temperature to stain live (green) and dead cells (red) respectively. After incubation for 15 min, the hydrogel fibers were rinsed for three times in PBS and imaged using a fluorescence microscope (Keyence BZ‐X700, Itasca, IL, USA). The live cells were imaged with excitation wavelength at 488 nm and emission wavelength at 499–537 nm, while the dead cells were imaged with excitation wavelength at 528 and emission wavelength at 617 nm. The images of live cells and dead cells were merged together using the analysis software (BZ-X Analyzer, Itasca, IL, USA).

3.2.6 Gene Expression Evaluation

RNA in the silk hydrogel fibers with 3% and 5% silk concentrations cultured in growth media for 1, 7 and 14 days at static state, and stretched for 24 h was isolated using the Qiagen RNeasy kit according to the manufacturer's directions. The sample

in a 2 mL microcentrifuge tube was flash froze in liquid nitrogen and homogenized for 5 mins in 600 μL lysis buffer to break up the cells. The homogenized samples were vortexed for 1 min and centrifuged at 4 °C in a micro-centrifuge at 13000 rpm for 15 mins. The supernatant was transferred to a column to collect the isolated RNA in a RNase-free collection tube through a set of centrifuges. The concentrations of the RNA were determined using the Nanodrop software. RNA was then reverse transcribed to cDNA using an Applied Biosystems High Capacity Reverse Transcription Kit. Quantitative real time polymerase chain reaction (qPCR) was applied to analyze and investigate expressions of RUNX2 (Hs 01047973_m1, Applied Biosystems, Foster City, CA), PPARγ (Hs 01115513_m1, Applied Biosystems, Foster City, CA) and CD90 (Hs 00174816_m1, Applied Biosystems, Foster City, CA), indicating the osteogenic fate, adipogenic fate and multipotency of hMSCs in the silk hydrogel, respectively. The control group was the hMSCs cultured on tissue culture plates, and GAPDH (Hs 02786624_g1, Applied Biosystems, Foster City, CA) was used as the house keeping gene.

3.2.7 Statistics

Differences between groups were examined for statistical significance using Student's t-test, one-way or two-way analysis of variance with Tukey post-hoc. Significance will be set at $p < 0.05$. Sample sizes were more than 3.

3.3 Results

3.3.1 Evaluation of Stiffness for Silk Hydrogel Fibers

The silk hydrogel fibers extruded from syringes were stable and stretchable thin fibers with 1 ± 0.18 mm diameter. The tensile properties of these silk hydrogels were determined through tensile tests in a PBS bath. Fibers were immersed in the growth media for 1, 7 and 14 days and then cut into 2 cm long sections. 4 tensile cycles up to 20% strain to eliminate artifacts and the followed fifth and sixth cycles were used to calculate tensile modulus within 10% strains. The final diameter was measured before starting the tensile tests. The hydrogel fibers fully recovered after six cycles of stretch. The stiffness measurements indicated that by varying the silk and H_2O_2 concentration, stiffness between 30 to 150 kPa can be obtained. The hydrogel fibers prepared with 5 wt% silk were higher than the hydrogel fibers with 3 wt% silk (**Figure 8b, c**). For 5 wt% silk (**Figure 8b**), the stiffness of 0.005% H_2O_2 concentration is higher than the 0.01% H_2O_2 concentration. However, for 3 wt% silk (**Figure 8c**), significant difference only occurred between 0.003% and 0.01% H_2O_2 concentration after 7 days culture. When the H_2O_2 concentration was 0.005%, the stiffness for both silk concentrations reached steady state at day 1, but if the H_2O_2 concentration changed to 0.003% and 0.01%, the stiffness increased in the first to second week.

3.3.2 hMSCs Encapsulation and Viability

In order to validate whether the silk hydrogel fibers were suitable for hMSCs encapsulation and growth, a live/dead stain was carried out for hMSCs loaded silk hydrogel fibers after culturing for 1, 14 and 21 days. The results on day 1 suggested that the hMSCs were alive and uniformly distributed inside the fibers. According to the live/dead stain on day 14 and day 21, the hMSCs maintained spherical shapes

with minimal extensions until day 14, and greater cell spreading and extensions observed on day 21 (**Figure 9**).

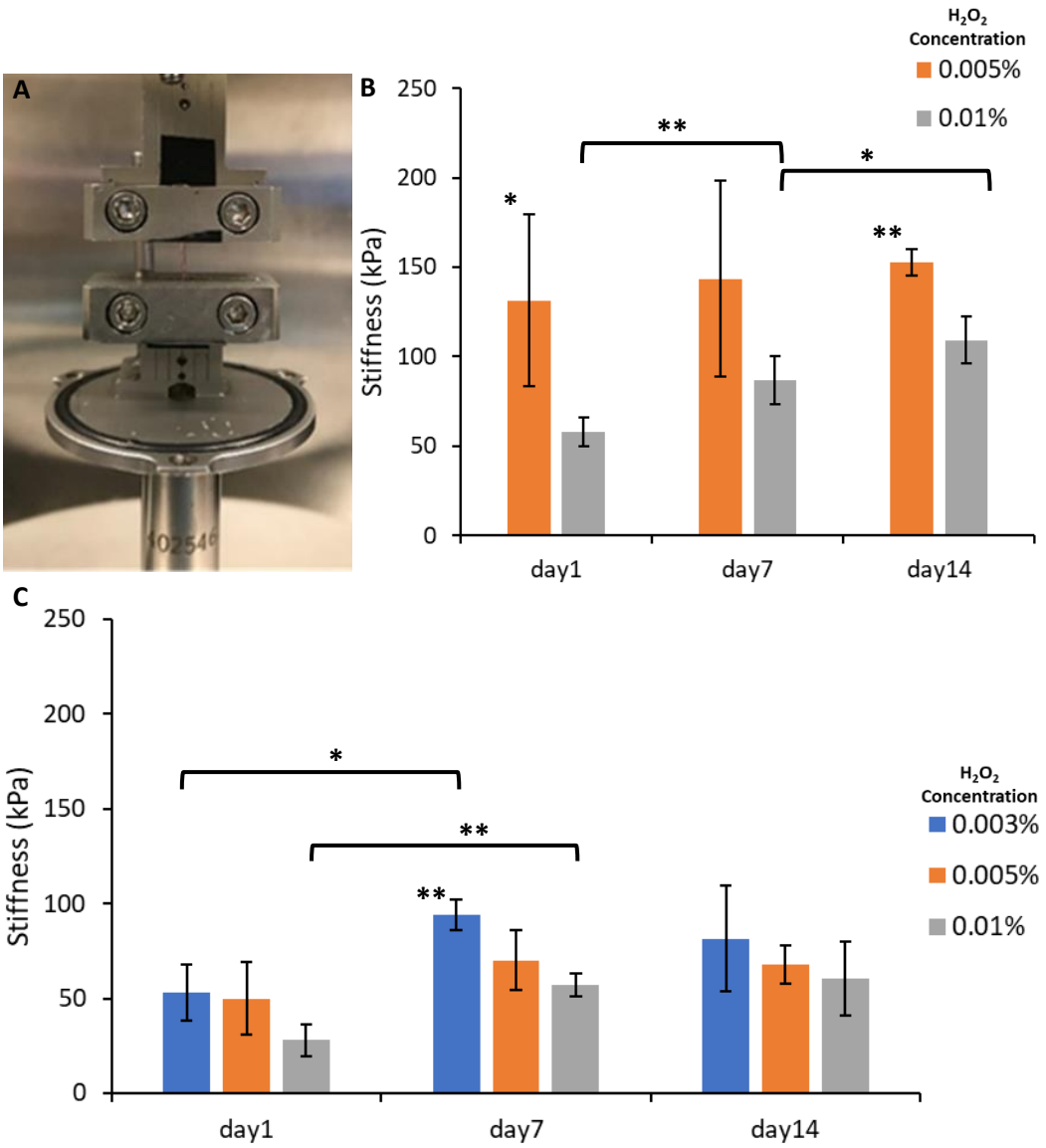

Figure 8. **a)** Applying tensile tests on silk hydrogel fibers using DMA. **b)** Stiffness of silk hydrogel fibers prepared with 5 wt% silk, 0.005% and 0.01% H_2O_2 concentration, after 1, 7 and 14 days culture. **c)** Stiffness of silk hydrogel fibers prepared with 3 wt% silk, 0.003%, 0.005% and 0.01% H_2O_2 concentration, after 1, 7 and 14 days culture. The results are shown as the mean values and standard deviations are presented as error bars. The statistically significance level was determined by p value using ANOVA: *, $P \leqslant 0.05$; **, $P \leqslant 0.01$, (n=3).

The metabolic activities of hMSCs in silk hydrogel fibers were determined by the Alamar blue assay. All the results were compared to the positive control group in which the hMSCs were seeded on a tissue culture plate. The Alamar blue assay after encapsulation for 1 day indicated that the metabolic activities for the hMSCs in silk hydrogels were nearly half of the hMSCs in tissue culture plates (**Figure 10a**). The metabolic activities of hMSCs in silk hydrogel increased after culturing for 7 days and reached a 1.68±0.04 and 1.7±0.11 fold increase of day 1 values for samples with 5% and 3%, separately (**Figure 10b**).

3.2.3 Gene Expression of hMSCs in Silk Hydrogel Fibers

The hydrogel fibers containing hMSCs were cultured either at static state or dynamic state where 10% strain and 1Hz cyclic stretch were applied using a flex cell plate for 24 h (**Figure 11**). The samples at static state cultured for 1, 7 and 14 days and the samples at dynamic state were collected for analyzing gene expressions of RUNX2, PPARγ and CD90. Gene expression was normalized to GAPDH and relative to controls whose values were set to 1. In silk hydrogel fibers made with 3 wt% silk, the PPARγ expression was upregulated by 2-fold and 11-fold on day 7 and day 14, respectively, and the RUNX2 expression also upregulated

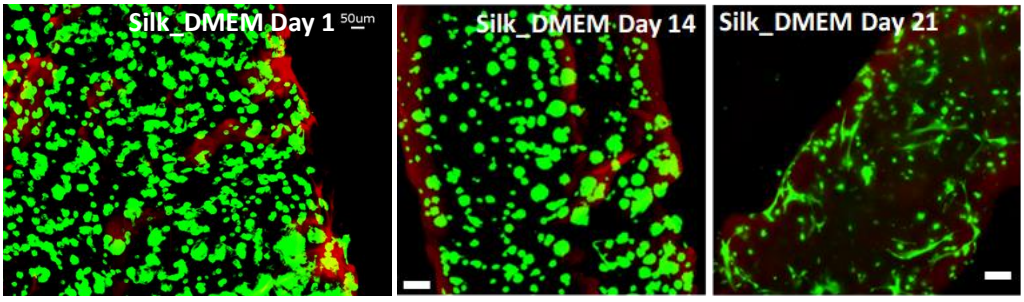

Figure 9. Live (green) and dead (red) stain of the hMSCs in the silk hydrogel fibers after 1 (scale bar: 50μm), 14 and 21 days (scale bar: 100μm) culture.

by nearly 6-fold and 13-fold on day 7 and day 14. While the CD90 expression downregulated to around 0.77-fold and 0.49-fold on day 7 and day 14 of the control condition. In silk hydrogel fibers made with 5 wt% silk, the PPARγ expression was also upregulated by 2-fold and 7-fold on day 7 and day 14, and the RUNX2 expression upregulated by nearly 7-fold and 8-fold on day 7 and day 14. Interestingly, the CD90 expressions were similar to the control condition on day 1 and 14 but upregulated to around 2-fold on day 7 of the control condition (**Figure 12a, b, c**). After applying cyclic stretching for 24 hours, all the gene expressions were upregulated even for CD90 compared to culturing at static state for 24 h, especially the RUNX2 expression, which showed no significant difference to the samples culturing at static state for 14 days (**Figure 12d, e, f**). The two-day ANOVA also suggested interactions between cyclic stretch and substrate stiffness on the gene expression of RUNX2 and CD90.

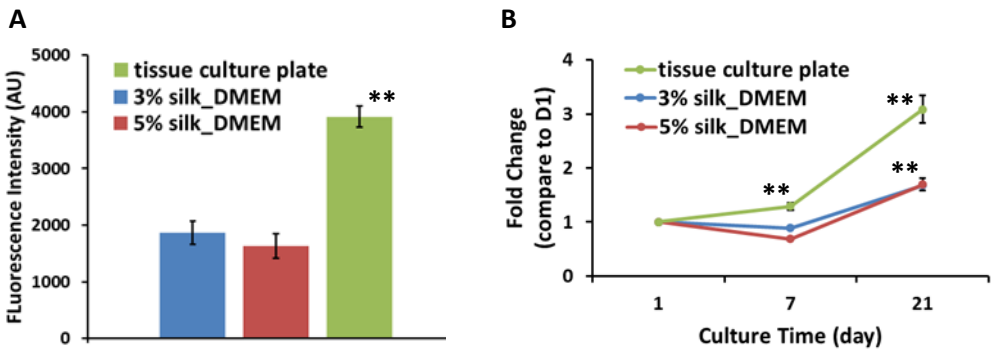

Figure 10. **a)** Survival of hMSCs encapsulated in silk hydrogel fibers prepared with 3 wt% and 5 wt% silk formed in DMEM compared to cells seeded on tissue culture plate tested by Alamar blue at day 1 post encapsulation. **b)** Cell proliferation in silk hydrogel fibers prepared with 3 wt% and 5 wt% silk formed in DMEM and tissue culture plate in 21 days tested by Alamar blue. The results are shown as the mean values and standard deviations are presented as error bars. The statistically significance level was determined by p value using ANOVA: *, $P \leqslant 0.05$; **, $P \leqslant 0.01$, (n=3).

3.4 Discussion

Understanding the effects of substrate stiffness and cyclic stretch on hMSCs fate is necessary for optimizing the biomaterial scaffold properties to support targeted long-term hMSCs differentiation *in vivo*. Silk fibroin, as a newly developed biomaterial, has been widely used in tissue regeneration [86, 87], drug delivery [88-90] and *in vitro* models. Mechanical properties, elasticity, biocompatibility and controlled biodegradation of silk fibroins are all valuable properties for implantation and tissue regeneration. Therefore, to optimize the design of implanted silk scaffolds loaded with stem cell, a silk system should be developed to investigate how substrate stiffness and mechanical stimuli affect hMSCs differentiation. Recently developed enzymatically crosslinked silk fibroin hydrogel was use in this project as the system due to its tunable mechanical properties, high elasticity and biocompatibility [6, 68].

The gelation of the silk solution was achieved through the formation of a tyrosine crosslinked network. This peroxidase reaction can be tuned significantly by varying tyrosine concentration (which can be treated as silk concentration), molecular weight (which is determined by the boiling time of silk fibroin), HRP and H_2O_2 concentration [6]. According to a previous study, the crosslinking efficiency decreased when the silk concentration increased, and the modulus will increase with increased silk concentration until a maximum value and then decrease [91]. In this project, stiffer hydrogels were found with 5% silk concentration compared to the 3% silk concentration, which suggested that 3% and 5% silk concentration is still within optimal range.

Figure 11. Silk hydrogel fibers are attached to tissue train plates. Cyclic stretch with 10% strain at different frequencies will be applied using flex cell plates.

During the gelation process, the H_2O_2 forms an oxyferryl center and a porphyrin-based cation radical to active HRP for undergoing followed reaction [92]. However, inhibition of HRP by higher H_2O_2 concentration would lead to lower crosslink density. Thus, when the crosslink density decreased, the modulus hydrogel also decreased. Stiffening of the initial crosslinked silk hydrogels with time has been found in several studies before due to the slowly self-assembles β-sheet secondary structure in silk [93, 94]. This process usually took several weeks. However, the stiffness of silk hydrogel fibers used in this project reached the steady state in only 1 or 2 weeks, or even in 1 day for samples with 0.005% H_2O_2 concentration. This was likely due to faster hydrogel water loss because of the higher surface to volume ratio of the thin fibers than a bulk of hydrogel. To further confirm this hypothesis, Fourier transform infrared spectroscopy (FTIR) should be taken to evaluate the ratio of β-sheet to random coil [93].

According to the mechanical properties evaluation, the silk concentrations of the hydrogel fibers used in this project were determined to be 3% and 5% to reach stiffness at around 60 kPa and 150 kPa. The concentration of H_2O_2 was chosen to

be 0.005% to eliminate the interference of stiffening on hMSCs' differentiation. Traditional surface seeding of hMSCs has been widely used for early drug discovery and screening. Compared to 2D matrices, 3D culture has been proved to be a more efficient way mimicking natural ECM environment. Differences of cell adhesion and signaling pathways were observed between 2D and 3D environment [95]. Here, we found that encapsulation of cells in silk hydrogel fibers enabled the uniform cell distribution from the center to the surface and prevented cellular gravity deposition. Discarding the cell loss during the encapsulation process, the surviving hMSCs were capable of long-term growth in the silk hydrogel fibers and showed increased metabolic activities and more cell spreading after culturing for two weeks.

Gene expression is a direct way to study early hMSCs differentiation. To investigate the multipotency of hMSCs in conditions with or without mechanical stretch, expression of CD90, a marker for a variety of stem cells, was measured. Decreased CD90 expression was found in both hydrogel fibers prepared with 3 wt% and 5 wt% silk after 1-week culturing at static state, suggesting reduced multipotency and possible entering of hMSCs differentiation. However, CD90 expression increased significantly after 24 h cyclic stretch compared to the static state regardless of the substrate stiffness. Scientists found that expression of CD90 in osteoblasts was maximal during the proliferation and early stage of maturation, and the expression decreased close to maturation [96, 97]. It suggested that hMSCs entering earliest stage of osteo-differentiation due to cyclic stretch.

PPARγ is a critical positive regulator for adipocyte formation and a negative regulator for osteoblast formation. Whereas, RUNX2 is an osteoblast-specific transcription factor. When hMSCs were cultured at static state, a significant increase in expression of PPARγ and RUNX2 was found over time in both silk hydrogel fibers prepared with 3 wt% and 5 wt% silk. Similar trends of PPARγ and RUNX2 expressions were also observed at dynamic state. It suggested that 24 h cyclic stretch promoted hMSCs entering osteo-differentiation and thus led to obvious upregulation of RUNX2, which was only observed in hMSCs after two weeks culture at static state. Although the final direction of hMSCs differentiation into osteoblasts or adipocytes is determined on activation of either RUNX2 or PPARγ, the mechanisms still haven't been fully developed. Recently identified Yes-associated protein/ transcriptional co-activator with PDZ-binding motif (YAP/TAZ) were found to interact with RUNX2 and PPARγ, suggesting their roles in switching between osteogenesis and adipogenesis [98, 99]. Therefore, the upregulation of both RUNX2 and PPARγ indicated that hMSCs was in a pre-osteoblast/adipocytes state, and the further differentiation of hMSCs would be determined through signaling transductions. Stiffness and mechanical stretch were varied from the surface to the center of silk hydrogel fibers. Therefore, encapsulated hMSCs might also differentiate into specific lineages, such as osteo-differentiation at stiffer sites and adipose-differentiation at softer sites.

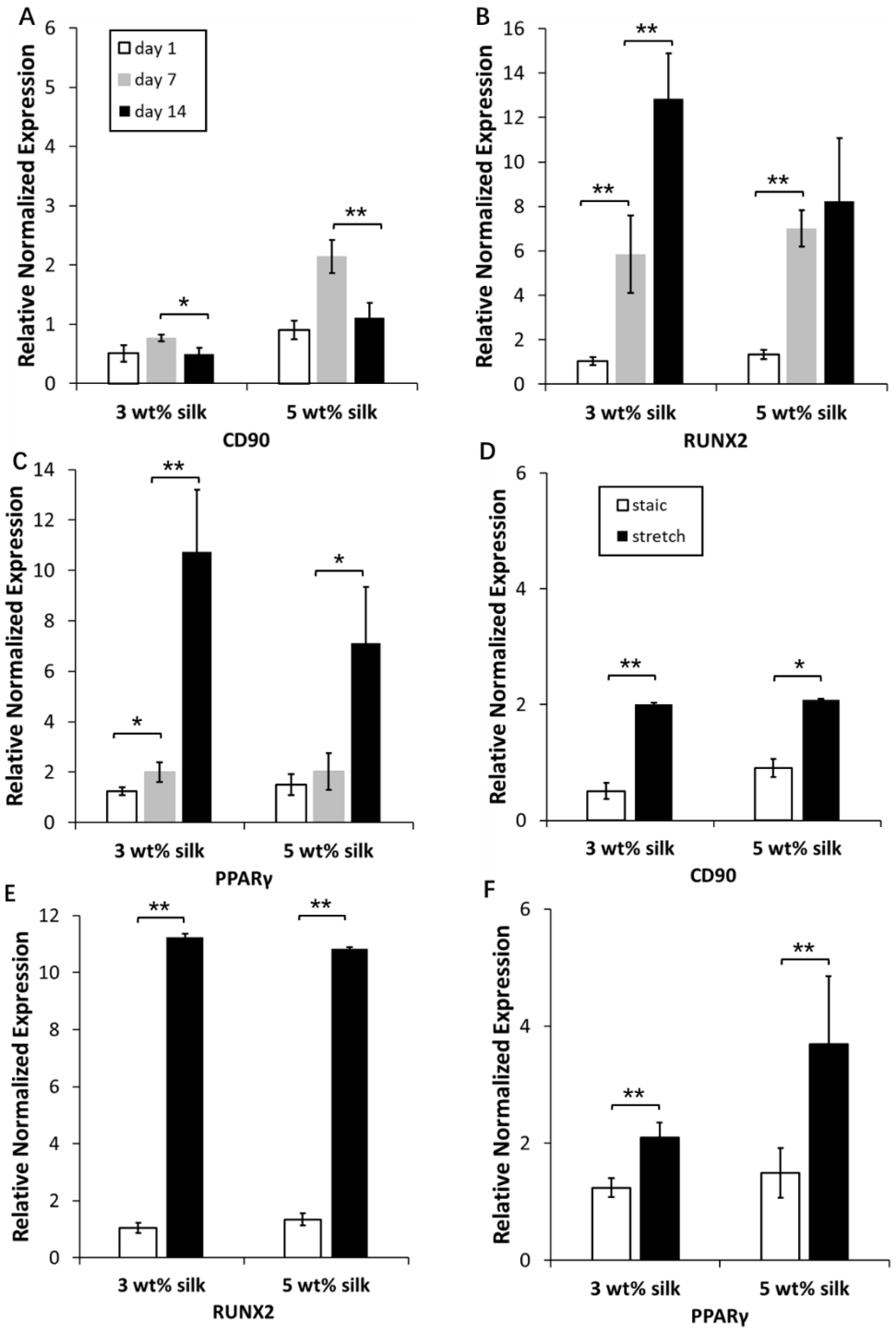

Figure 12. Gene expression of CD90, RUNX2, PPARγ in hMSCs encapsulated in silk hydrogel fibers with 3 wt% and 5 wt% silk formed in growth media for 1, 7 and 14 days at static state (**a, b, c**) or stretched for 24h at 10% stain and 1Hz (**d, e, f**). The control group is the hMSCs cultured on tissue culture plates. The results are shown as the mean values and standard deviations are presented as error bars. The statistically significance level was determined using ANOVA: *, $P \leqslant 0.05$; **, $P \leqslant 0.01$, (n=3).

Although these results are not sufficient for finding a conclusion on the effects of substrate stiffness and cyclic stretch on hMSCs' fate in silk hydrogel system, they did confirm the possibility for using this silk hydrogel fiber as a 3D system for investigating the long-term effects of mechanical and biochemical cues on hMSCs' differentiation. The study suggested that encapsulating hMSCs in silk hydrogel fibers over 50 kPa led to potential hMSCs differentiation, and application of cyclic stretch further induced expression of osteoblast-specific transcription factors, while inhibiting expression of adipocyte-specific transcription factors. In the future, long-term studies on gene expression, ECM remodeling and several related signaling pathways would provide more information for explaining effects of different cues on hMSCs' fate, and thus optimize the composition and properties of silk biomaterials scaffolds to direct hMSCs differentiation both *in vitro* and *in vivo*.

Chapter 4 – Generation of a Vascularized, Anisotropic Silk Scaffold for Tissue Regeneration

4.1 Introduction

Tissue failure due to cell death or severe damages is one of the major life-threatening diseases [12-14]. Although several treatments such as synthetic prosthesis, mechanical devices and transplantation have been explored to repair or replace damaged tissue, there are still challenges including immature post-surgery function, unwanted immune responses and fewer donors available for transplantation. A functional engineered tissue construct containing 3D scaffolds and stem cells is one of the major techniques being explored for repairing damaged tissue. Tissue engineered constructs mimic the structure and functions of natural tissue with application of mechanical and biochemical cues to regenerate specific tissue based on cell-cell and cell-matrix interactions. To achieve the clinical utility and improvement for tissue regeneration treatment, a critically sized tissue engineered construct needs to be at several millimeters scales with a dense vascular network and immediate vascular anastomosis. After implantation, sufficient oxygen and nutrients can only reach a distance of 100-200 μm from the capillary due to the diffusion limit. Highly functional tissues, especially liver and cardiac tissue, are very sensitive to low oxygen levels and thus, direct surgical anastomosis with immediate perfusion of vascularized tissue is necessary for cell survival.

Vascular networks can be generated in collagen, alginate and gelatin hydrogels using different techniques [27-29]. However, a major challenge using hydrogels, is

not being able to achieve an anisotropic structure, which is important for cells alignment in several natural tissues such as neural and heart tissue. Anisotropic structures in tissue engineered constructs are necessary to achieve various anisotropic functions including anisotropic diffusion, mechanics and electrical conduction, which are important in heart, muscle, bone or neural tissue. Anisotropic diffusion of macromolecules and nanoparticles through the scaffold plays an important role in biological activities. Stylianopoulos, T *et al*. have studied the anisotropic diffusion of macromolecules and nanoparticles in oriented collagen fibers using a mathematic model in 2010. The results showed that the overall diffusion coefficient is relatively similar in the anisotropic networks, however, the directional components of the diffusion coefficient varied with different degrees of fiber alignment, particles sizes and volume fiber fraction [100]. Anisotropic mechanics and electrically conduction also contribute to muscle contraction and spontaneous heart beating. For example, alignment of cardiomyocytes and anisotropic distribution of cell-cell junctions have potential effects on action potential propagation and generation of contractile force [101, 102]. Therefore, tissue engineered constructs should be able to recapitulate the anisotropic structures of the natural tissue they intend to replace.

In comparison to hydrogel-based systems, the direction of the fibers in sponges can be well organized and maintain their structural integrity during and post-surgery. Synthetic polymers such as polyurethane and PLLA can be used for generating anisotropic sponges in tissue engineering [103, 104]. However, the limitations in biocompatibility and biodegradation remains problems for long-term implantation.

Freeze-drying is one of the frequently used techniques in introducing anisotropic structures, which can be used in making anisotropic collagen scaffold [105]. Although the collagen scaffold has advantages in biocompatibility, the difficulties in further modification of mechanical and biochemical properties need to be taken into consideration.

Silk fibroin, an extensively studied biomaterial in tissue engineering and regenerative medicine [56], has shown advantages in good biocompatibility, tunable mechanical and biophysical properties, and controllable degradation rate in several studies [57-59]. The silk fibroin can also be fabricated into various formats including fiber, film and scaffold, enabling the wide application of silk in the biomedical field [60]. One type of silk sponge generated through a freeze-drying process can achieve both isotropic and anisotropic structures, which has been well demonstrated for its applications in tissue engineering. For example, a biodegradable anisotropic silk-ECM cardiac patch has been established previously. The patch mimicked the anisotropy of heart tissue while cECM improved cell infiltration and vascularization [61].

In this present study, a silk-based tissue engineered construct will be generated to recapitulate anisotropic structures of natural tissue such as muscle, heart, neural etc.. Branching networks will be incorporated into the constructs for vascularization and surgical anastomosis. The newly formed anisotropic silk-based sponge with branching networks is expected to contribute in improving tissue regeneration with ability to seed stem cells and integrate mechanical and biochemical cues for specific stem cell differentiation.

4.2 Methods

4.2.1 Silk Solution Preparation

Silk solution was made as described in the method of Chapter 3, however, the boiling time for the silk cocoons was 30 min.

To prepare the concentrated silk solution (around 15% silk concentration), 20 mL 6% to 8% silk solution were injected into a Slide-a-Lyzer dialysis cassette (3,500 molecular weight cut off). The dialysis cassette was put in a chemical hood at room temperature for 12 to 24 hours until the volume of the solution decreased to 8-10 mL to concentrate the silk solution. The concentrated silk solution was removed from the dialysis cassettes and the silk concentration was determined as described above. The final silk solution yielded 14% to 20% (w/v).

4.2.2 Gelatin Mold Fabrication

The channels in a silk scaffold were generated using gelatin. Solidworks ® software ver. 2015 (SolidWorks Corporation, Concord, MA, USA) was used to generate a 3D parametric CAD model, which is a complementary shape of the half channels cut along the long axis. A milling machine was used to fabricate the CAD model on a high-density polyethylene (HDP) sheet. Polydimethylsiloxane (PDMS) was poured onto the HDE mold and placed in a 60°C oven for 4 hours for curing. Two PDMS molds were combined to form a whole channel. Gelatin solution was made by dissolving 5 g gelatin powder (Sigma, United States) into 20 mL 60°C distilled water. The 20% (w/v) gelatin solution was injected into the PDMS mold and left in -20°C freezer for 5min to induce faster curing. The cured gelatin mold was pulled

off from the PDMS mold and lyophilized for 24 hours to shrink the diameter of the mold to half. The gelatin mold was dipped into 12% silk solution followed with methanol to induce β-sheet formation of silk fibroin. This process was repeated for three times and water annealed for 4 hours later to form a uniform silk film around the gelatin mold. The silk film was acted as the 'channel wall' to prevent the loss of seeded Human umbilical vein endothelial cells (HUVECs).

4.2.3 Anisotropic Scaffold Assembly

A HDP made squared container with a metal bottom located on a box of dry ice and 98% ethanol was used to make the anisotropic silk scaffold with channels. The gelatin mold was fixed in the middle of the container and 10-20 mL 3% silk solution were poured into the container (**Figure 13b**) to immerse the gelatin mold. The freezing agent froze the metal bottom and in turn froze the silk solution to create anisotropic silk fibers around the gelatin mold. The frozen silk was then lyophilized and autoclaved. The silk scaffold was immersed in 60°C distilled water to melt the gelatin out and finally generate an anisotropic silk sponge with channels (**Figure 13a**).

4.2.4 Microstructure Observation using Scanning Electron Microscope (SEM)

The silk scaffold was dehydrated in a series of graded ethanol extractions. The dried silk scaffold was cut from the middle of channels along the long edges using razor blades. SEM (Supra55VP, Zeiss) was used to observe the microstructure of the silk scaffold and channels coated with gold/palladium for 120 secs before SEM observation.

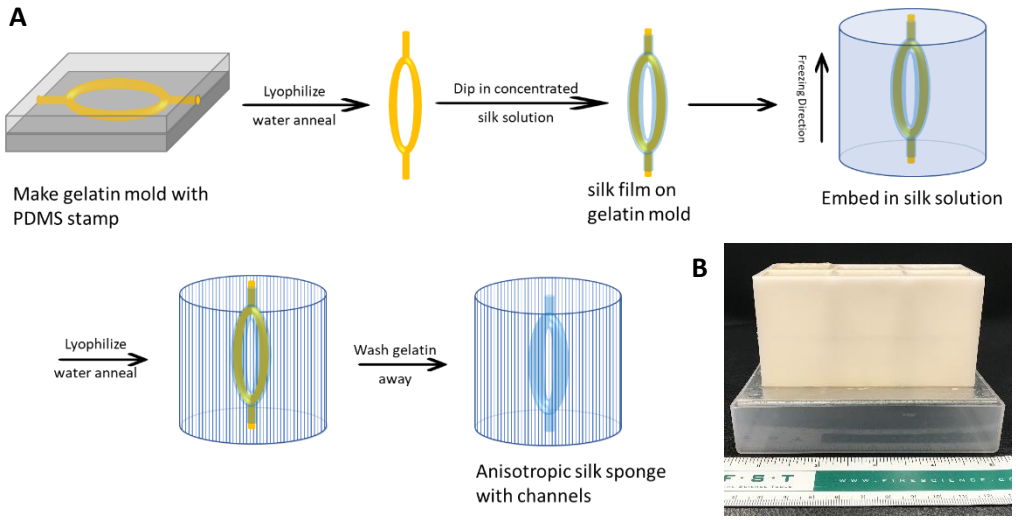

Figure 13. **a)** Schematic of silk scaffold making. **b)** Device of making the silk scaffold

4.2.5 Diffusion Coefficient Measurement

The diffusion coefficients in the anisotropic silk scaffold were measured using a Macroscope (Olympus MVX10 microscope using cellSens Dimension software (version 1.8.1, Olympus Corporation)). The measurement of diffusion coefficients followed the method described in a previous paper [106]. Briefly, the anisotropic silk sponge was trimmed into thin slices (0.1-0.2 mm) and immersed in distilled water overnight to reach equilibrium. 3 kDa and 40 kDa were chosen as the two tested molecular weights to mimic small molecules such as growth factors and large molecules such as proteins in the tissue. 2 μL 1 mg/mL 3 kDa or 40 kDa fluorescein isothiocyanate-dextran (FITC-dextran) was pipetted in the middle of sponge slices and a sequence of fluorescence images with 0.3 s intervals were taken to record the FITC-dextran diffusion. The fluorescent intensity maps at major axis (along the aligned fiber) and minor axis (perpendicular to the aligned fiber) of each image

were plotted. Gaussian fits of these curves were performed using Matlab following the equation:

$$\mathrm{I(x,y,t)} = E(t)\exp\left[-\left(\frac{x^2}{{\gamma_x}^2}+\frac{x^2}{{\gamma_y}^2}\right)\right]$$

The curves of $\frac{{\gamma_x}^2}{4}$ or $\frac{{\gamma_y}^2}{4}$ with respect to time (s) was plotted and the slopes were considered to be the diffusion coefficients. Isotropic silk sponge slices were used as the controls to directly visualize the difference between isotropic diffusion and anisotropic diffusion.

4.2.6 Cell Seeding and Immunohistochemical Staining

HUVECs were cultured in optimized growth media (EGM-2) consisting of Endothelial Basal Medium-2 supplemented with EGM-2 Bullet kit (PromoCell). Cells were cultured at 37 °C, 5% CO_2/95% air, and 95% relative humidity. Cell culture medium was changed every two days, and cells were passaged at approximately 80% confluence using Trypsin-EDTA (0.25% trypsin with 1 mm EDTA·4Na) and frozen in cryogenic media consisting of growth medium supplemented with 10% (v/v) dimethyl sulfoxide (DMSO).

To determine the protein used to coat the channel walls, silk films were made in 24 well tissue culture plates and coated with 100 μg/mL type I collagen, fibronectin and type IV collagen separately. HUVECs were seeded on the silk films at the density of 5,000 cells/cm^2 and cultured at 37 °C, 5% CO_2/95% air, and 95% relative humidity for 7 days. The silk films were stained with DAPI for cell counting at day 3 and day 7. The junctions between endothelia cells were determined through VE-

cadherin stain at day 7. The images were analyzed using Cellprofiler to count the cell numbers and positive VE-cadherin expression, which was calculated as the ratio of number of cells expression VE-cadherin over the total number of cells in an image.

Before seeding the HUVECs, the channel walls were coated with 500 μg/mL collagen-I to improve the HUVECs adhesion. 20 μL suspension of HUVECs with the density at 5×10^6 cells/mL were pipetted into the channels and incubate at 37 °C for 1 hour until the HUVECs attached to half of the channel walls. The silk scaffold was then turned over and HUVECs were seeded on the other half of channel walls following the same process. The silk scaffold was cultured in the growth medium which was changed every day.

The silk scaffold was fixed in a 4% formaldehyde solution in PBS for 15 mins at room temperature, and permeabilized with 0.05% Triton X-100. After blocking with 1% bovine serum albumin (BSA) and 5% donkey serum in PBS, the silk scaffold was cut into half from the middles of the channels and incubated with the mouse anti-VE-cadherin (1:100) overnight at 4°C, followed by detection using Alexa Fluor-coupled secondary antibodies (Life Technologies). Nuclei were counterstained using DAPI (Carl Roth) added at the last 5min during incubation with the secondary antibody to prevent the high background signals from the silk fibroin. The images were taken with a fluorescence microscope (Keyence BZ - X700, Itasca, IL, USA).

4.2.7 COMSOL Simulation

COMSOL Multiphysics (COMSOL Inc.) was used for building a simplified mathematical model representing the anisotropic silk scaffold with a straight channel through the middle. Physical equations used in prior bioreactor simulation research were modeled through COMSOL 5.2's "Reacting Flow in Porous Media" module; fluid mechanics were described by the continuity equation and Navier-Stokes equations, including the solutions in porous media developed through incorporation of Darcy's Law, while the convection-diffusion equation describes the transport of dissolved oxygen by both moving fluid and diffusion down its concentration gradient [107, 108].

To incorporate biomass behavior, and the connected equations for describing oxygen consumption, COMSOL's module for general partial differential equations was used in conjunction with a modified form of Fisher's equation:

$$\frac{dC}{dt} = [H(S - S_h)\,\mu_R \frac{S}{Km+S} - k_d]C\,(1 - \frac{C}{C_{max}}) + \nabla \cdot (D_{eff,\,C}\nabla C)$$

which incorporates terms intended to represent biomass growth, death, and diffusion [108, 109]. C represents the cell density [cells/m^3], S the substrate (oxygen) concentration [mol/m^3], H is the Heaviside step function as approximated through COMSOL's smoothed step function options, which returns 1 if the input is positive and 0 otherwise, S_h a threshold concentration of oxygen intended to prevent oxygen consumption at miniscule levels of substrate from causing negative solutions, and K_m is a Michaelis-Menten oxygen concentration constant which decreases cell growth rate at sufficiently low oxygen concentrations as in the Monod equation: $\frac{dC}{dt} = \mu_R \frac{S}{Km+S}\, C$ (3) [109]. The specific replication rate and cell death rate are represented by μ_R and k_d, respectively [cell/s]. C_{max} is a parameter

calculated using approximate cell volume and the scaffold porosity and represents the maximum density at which further biomass growth is prevented by physical limits. The effective diffusion coefficient $D_{eff,\,C}$ [m^2/s] describes the diffusion rate of cells throughout the scaffold down their concentration gradient and was assumed to be similar to COMSOL's diffusion approximation for porous media where the relevant diffusion coefficient multiplied by $\varepsilon_p^{3/2}$, where ε_p is scaffold porosity. The scaffold's porosity and permeability (κ) were assumed to decrease with increased cell concentration as in previous research accounting for cell growth: $\varepsilon_p = \varepsilon_{p0} e^{\frac{-Vcell(C_{total})}{\varepsilon_p}}$ and $\kappa = \kappa_0 e^{\frac{-Vcell(C_{total})}{\varepsilon_p}}$ [54]. C_{total} is a sum of local biomass density and the local density of HUVECs where the channel layer is, as the HUVECs were assumed to provide a similar barrier to diffusion and fluid motion.

To model oxygen consumption, the reaction equation, describing oxygen sink behavior in the convection-diffusion equation, was made to incorporate both the custom biomass and consumption behavior assumed for a constant layer of HUVECs:

$$R = -R_{HUVEC} C_{HUVEC} \frac{S}{Km\ S} H(S - S_h) H(\frac{wchannel}{2} + w_{HUVEC} - x) - R_{ESC} C \frac{S}{Km\ S} H(S - S_h)$$

R_{HUVEC} and R_{ESC} denote values for oxygen consumption rates by HUVECs and embryonic cells, where the latter was assumed for the growing biomass. The Michaelis constant K_m was assumed to produce consumption-limited behavior at the same concentration as growth would become inhibited. C_{HUVEC} describes an assumed constant density of the HUVEC layer; the HUVEC population is physically defined by the second step function in the above equation, which stops

accounting for HUVEC-related oxygen consumption beyond a fixed distance from the channel wall ($wchannel$).

4.2.8 Statistics

Differences between groups were examined for statistical significance using Student's t-test. Significance will be set at $p < 0.05$. Sample sizes were more than 3.

4.3 Results

4.3.1 Anisotropic Silk Scaffold Fabrication and Microstructure

Following the steps described in the methods, the branched PDMS molds (**Figure 14a**) and gelatin molds (**Figure 14b**) for the channels were successfully made. The surfaces of the molds were smooth, and the diameters of the gelatin mold decreased to half of the originals after lyophilization without changes on shapes. A thin and transparent silk film was coated on the gelatin mold by dipping the mold repeatedly in concentrated silk solution and methanol for 3 times. The 3% silk solution froze along the direction of the branched channels. After lyophilization and sterilization and β-sheet formation through autoclave, an anisotropic silk sponge was formed with the gelatin mold in the center. The gelatin can be fully washed away with 60°C water and left with branched channels in the silk sponge.

Water with red dye was injected through the inlet of the channels and confirmed fluent fluid flow through the channels. After injecting the water with red dye for 5 mins, the silk scaffold was cut into half from the center of the channels along the

direction of fluid flow. The images showed that the whole channels were stained to red. The surrounded silk sponge was still whitish suggesting no diffusion of water from the channels into the sponges due to fully silk coating around the channels (**Figure 14c**).

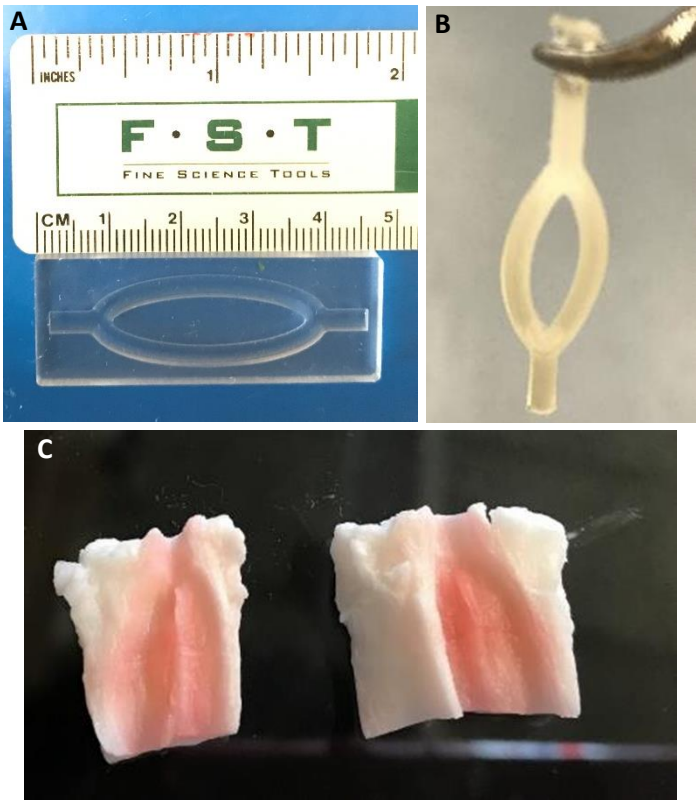

Figure 14. The pictures of **a)** Plastic and PDMS molds, **b)** gelatin mold, lyophilized gelatin molds coated with silk films and **c)** a silk scaffold with channels

The microstructures of the silk fiber alignment and the silk film made channel wall were observed using SEM. All the silk fibers were aligned along one direction to form an anisotropic silk sponge (**Figure 15a**) and no gaps were found on the channel walls made with concentrated silk (**Figure 15b**). The thickness of the

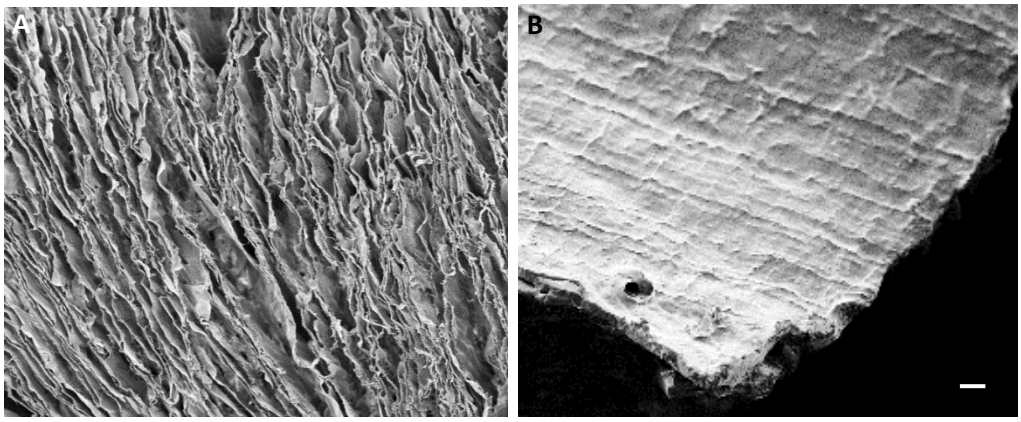

Figure 15. The SEM images of **a)** aligned silk fibers, Scale bar: 100μm and **b)** channel walls. Scale bar: 20μm

channel wall can be adjusted by the changing the concentration of the silk solution and the dipping times of the gelatin mold into the silk solution.

The direction of the silk fiber alignment can be directed by changing the freezing direction. Two types of silk sponges were made with silk fiber alignment either along (**Figure 16a**) or perpendicular (**Figure 16b**) to the channels. In order to observe the directions of water diffusion, pores were made on the channel walls by mixing 1% polyethylene glycol (PEG) into the concentrated silk solution. After injecting the water with red dye, the directions of the water diffusion were shown to follow the silk fibers alignment.

4.3.2 Anisotropic Diffusion Evaluation

Once the anisotropic structures have been confirmed in the silk sponges. Further analysis on the diffusion coefficients in the anisotropic sponges were measured according to a previous published method [106]. Because the dextran diffused faster in the silk sponge than the hydrogel, small time intervals were used to capture a sequence of images.

The fluorescent images showed that in isotropic silk sponges, FITC-dextran diffused uniformly to all the directions forming a circular shape (**Figure 17a**). However, in anisotropic silk sponges, FITC-dextran diffused faster along the fiber alignments and slower perpendicular to the fiber alignments and formed a spindle shape (**Figure 17b**).

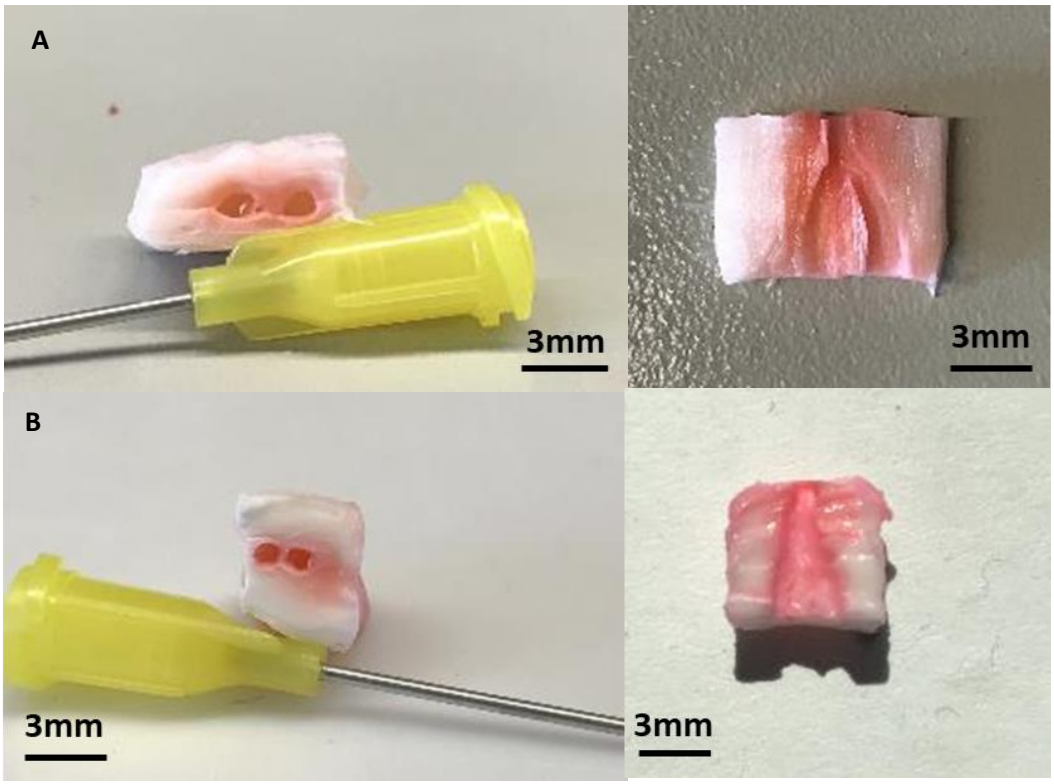

Figure 16. The fluid diffusion from channels to the surrounded areas in the silk scaffold with fibers **a)** aligned with the channels or **b)** perpendicular to the channels.

To statistically measure the anisotropic diffusion coefficients, fluorescent density maps on major and minor axis were plotted with respect to the distance. The density profiles were fitted with Gaussian curves in Matlab to obtain the values of $\frac{\gamma^2}{4}$ at different time points (**Figure 18a**). The values of $\frac{\gamma^2}{4}$ were then plotted with respect to the times and the diffusion coefficients were determined as the tangent of the $\frac{\gamma^2}{4}$-

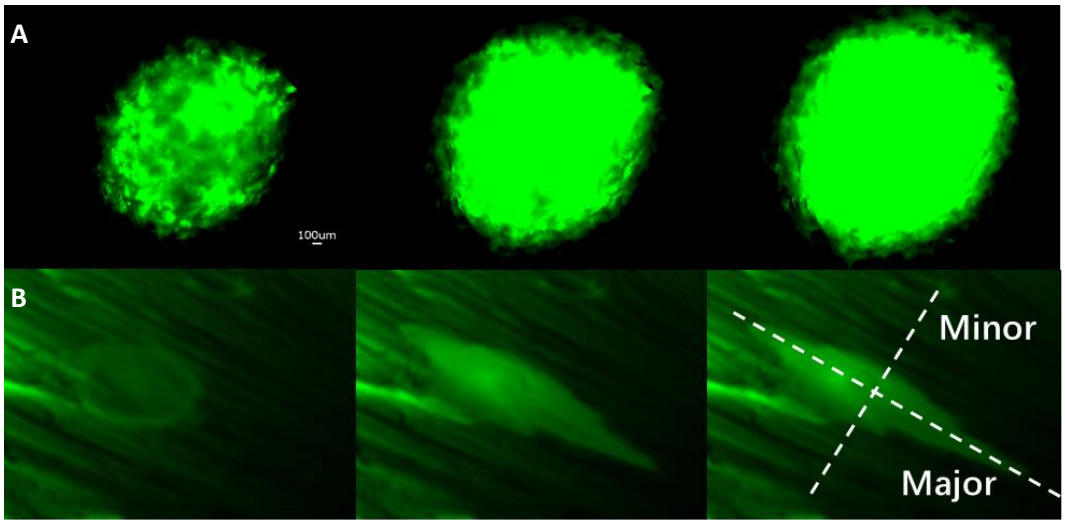

Figure 17. Sequence of images taken after the injection of 3kDa FITC-dextran in **a)** isotropic and **b)** anisotropic silk sponge with 0.3 s interval (scale bar 100 m). The major axis represents the direction along the fiber alignment and the minor axis represents the direction perpendicular to the fiber alignment.

time curves. For both 3 kDa and 40 kDa FITC-dextran, the diffusion coefficients of the major axis were higher than the minor axis. However, 40 kDa FITC-dextran diffused slower than the 3 kDa FITC-dextran in the anisotropic silk sponges. The diffusion coefficients of 3 kDa FITC-dextran on the major and minor axis were $(7.78 \pm 1.04) \times 10^{-6}$ cm^2/s and $(0.83 \pm 0.08) \times 10^{-6}$ cm^2/s (**Figure 18b**). The diffusion coefficients of 40 kDa FITC-dextran on the major and minor axis were $(1.39 \pm 0.12) \times 10^{-6}$ cm^2/s and $(0.41 \pm 0.01) \times 10^{-6}$ cm^2/s (**Figure 18c**).

4.3.3 Endothelialization

The first step for vascularization was to achieve endothelialization of the built-in channels in the silk scaffolds. HUVECs before passage number 4 were used for the endothelialization. Before seeding HUVECs in the channels, the channels need to be coated with specific proteins to promote the HUVECs adhesion and extension and thus improve the confluent HUVEC layers formation. To determine the most efficient protein to use for coating channels, 3 of the most abundant ECM proteins in the natural basal membrane: type I collagen, fibronectin and type IV collagen were evaluated for their efficacy in supporting cell proliferation and endothelial cell junction formation.

Silk films coated with 100 μg/mL type I collagen, fibronectin and type IV collagen separately were used to determine the best choice of coating protein to enhance HUVECs' proliferation and junction formation. The results indicated significant cell proliferation on all the coated silk films. But the silk films coated with type I collagen showed significant higher cell numbers than type IV collagen and fibronectin coated silk films on day 3. After 7 days culture, cell numbers on both type I collagen and fibronectin coated silk films were significant higher than the silk films coated with type IV collagen (**Figure 19a**). Both type I collagen and fibronectin coated silk films also achieved significantly more junction formation between HUVECs on day 7 compared to type IV coated silk films (**Figure 13b**). Therefore, type I collage was determined to be the best choice of protein to be used for coating channels.

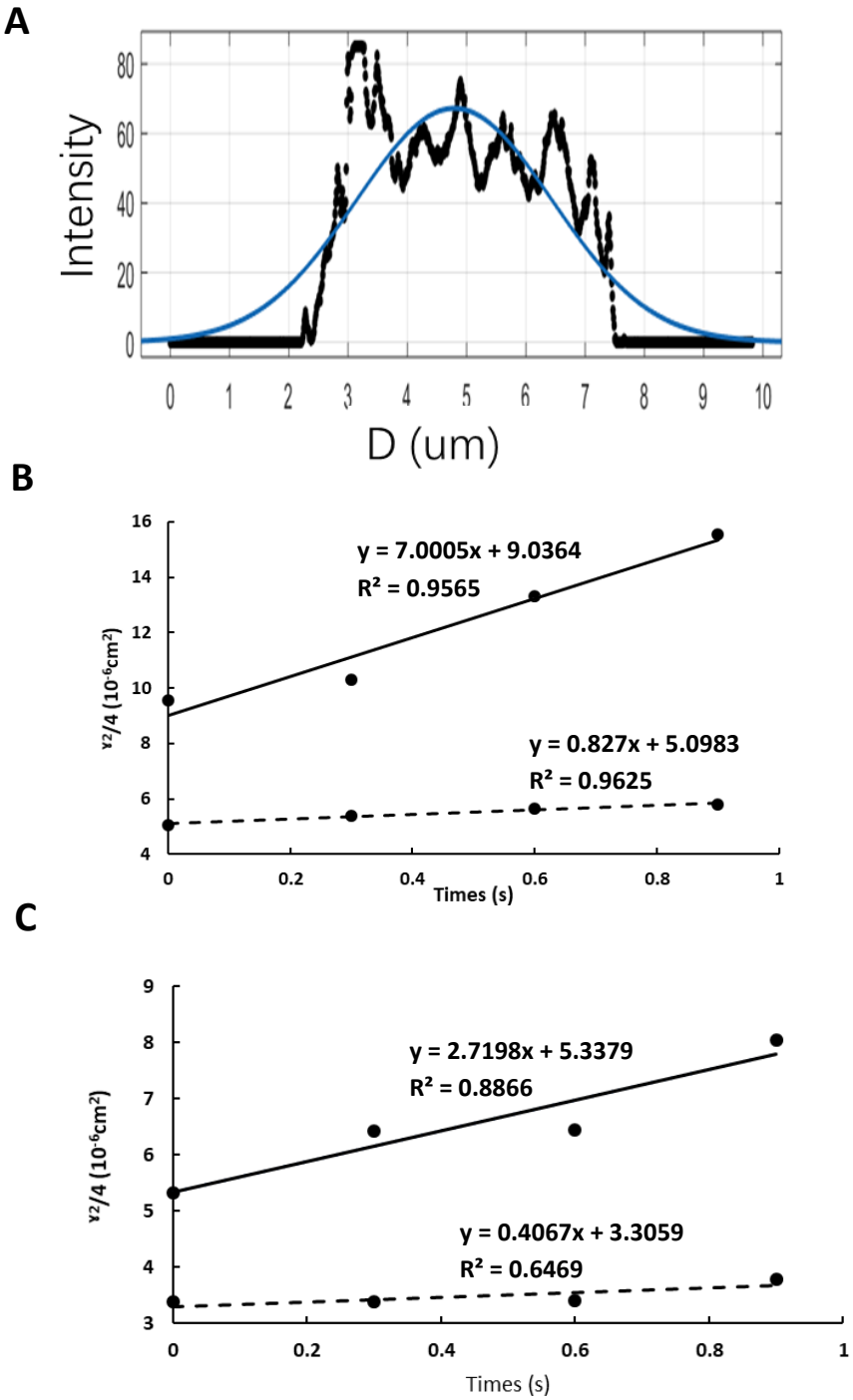

Figure 18. **a)** Fluorescence intensity profiles (black) extracted at t = 0.3 s along major axis are fitted with gaussian curves (blue). **b)** The values of diffusion coefficients of 3 kDa FITC-dextran at major (solid line) and minor axis (dash line) were estimated from the $\frac{\gamma^2}{4}$ versus time curves. The equations and values of R^2 were displayed beside fitted lines. **c)** The values of diffusion coefficients of 40 kDa FITC-dextran at major and minor axis were estimated from the $\frac{\gamma^2}{4}$ versus time curves.

A straight channel in the silk scaffolds were coated with 500 μg/mL type I collagen and seeded with HUVECs. The silk scaffold was flip upside down one during the HUVECs seeding process to seed the HUVECs uniformly around the channel. A

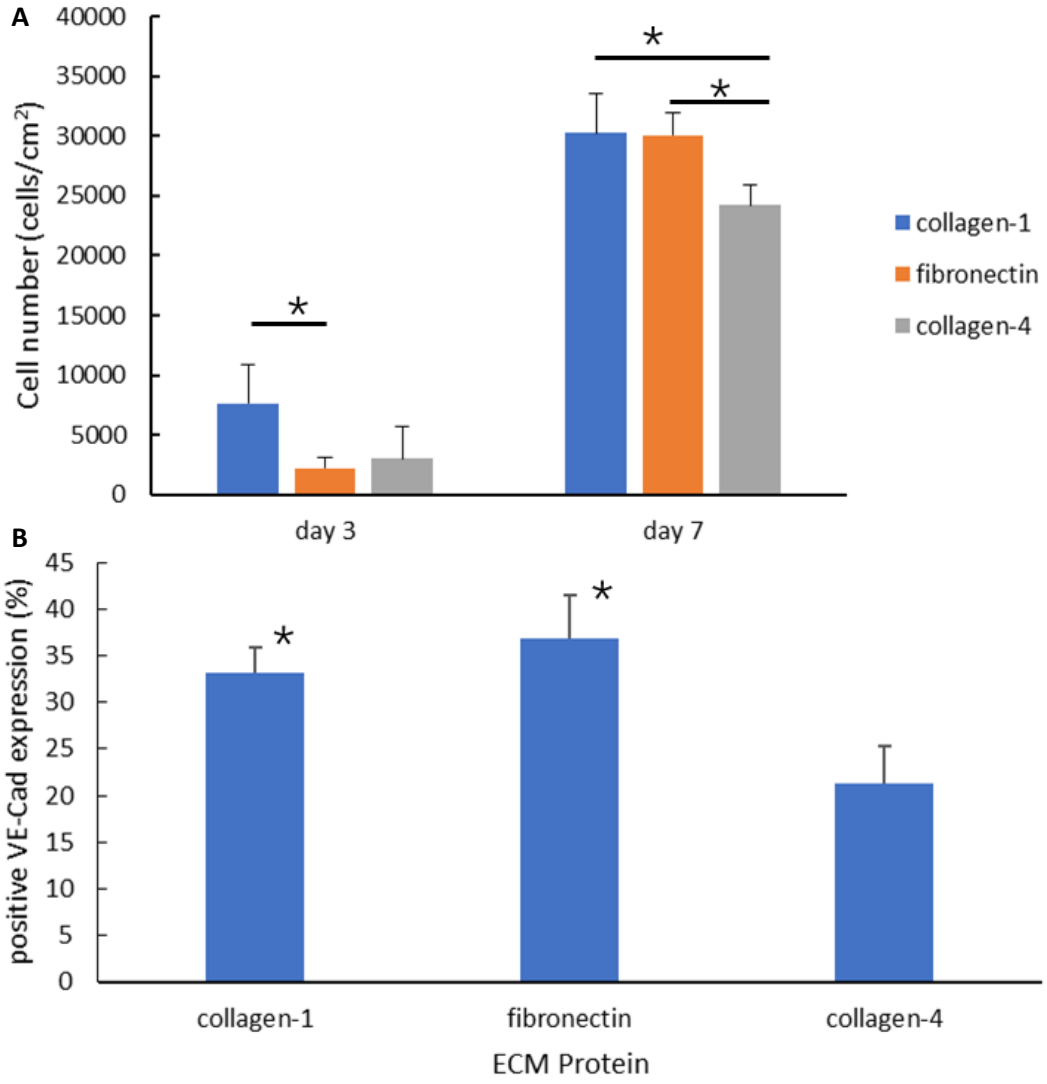

Figure 19. **a)** HUVECs numbers on collagen-1, fibronectin and collagen-4 coated silk films after culturing for 3 and 7 days. **b)** formations of endothelial cells junctions on collagen-1, fibronectin and collagen-4 coated silk films after culturing for 7 days. The results are shown as the mean values and standard deviations are presented as error bars. The statistically significance level was determined by p value using ANOVA: *, P $\leqslant$ 0.05; **, P $\leqslant$ 0.01, (n=3).

confluent HUVECs layer was observed on the channel and maintained until day 7 (**Figure 20a, b**). The HUVECs could also be seeded into branched channels, but the cells didn't reach higher confluency after 3 days culture (**Figure 20c**).

4.3.4 Simulation

In order to better understand the biological environment in the silk scaffold and thus optimize the design of the silk scaffold, COMSOL was used to simulate the changing of oxygen concentration (**Figure 21a, b**) and biomass growth (**Figure 21c, d**) in the silk sponge around the channels. The model was simplified to a squared silk scaffold with a straight channel through the middle of it. A confluent HUVEC layer was on the side of the channel and cardiac fibroblasts were seeded in the silk sponge. 5 mm and 10 mm wide silk scaffold was used for the simulation. The fresh media flew from the inlet to outlet of the channel. According the results of the running the model simulation, after culturing for 2 h, only the area within 2 mm from the channel remained normal oxygen concentration. The areas near the outlet or over 2 mm away from the channel are hypoxia regions. Due to the limitation of oxygen, the hypoxia regions were also where the lower biomass growth occurred compared to the region with normal oxygen concentration.

4.4 Discussion

In the recent years, with the increased demands of clinical treatment in healing injured tissue and replacing failed organs, development of complex engineered tissues or even organs for transplantation becomes a potential revolution of clinical treatment for tissue failure. However, many obstacles still need to be overcome to

meet clinical requirements. Recapitulation of the natural microstructures for specific tissue through a tunable tissue engineered construct and providing sufficient oxygen and nutrients to the entire engineered constructs are considered to be two of the major problems.

In natural tissue, the structures of many tissues are anisotropic and aligned following specific direction. For example, the structure of native myocardium is composed of several layers with parallel myocardial and collagen fibers and thus achieved anisotropic cell-cell junctions relating to electrical conduction [101, 102]. The alignment of each layer varies slightly with a small angle [110, 111]. The native bone tissue is also an anisotropic material which lead to different behaviors when the load was applied at different directions. For instance, the bone tissue, mechanical loading is generally applied in the longitude direction rather than the load being applied to the bone surface [112].

The silk-based construct generated in this project successfully recapitulate the anisotropic structures of nature tissue. The orientation of the silk fibers can be well controlled by the freezing direction. To match the anisotropic structures of specific tissue, the freezing direction can be maintained unchanged during the process or changed slightly at each layer to achieve different alignments in multi-layers. The stiffness of the silk sponge can also be tuned to match the specific stiffness of natural tissue with changes on molecular weight of silk fibroin or the concentration

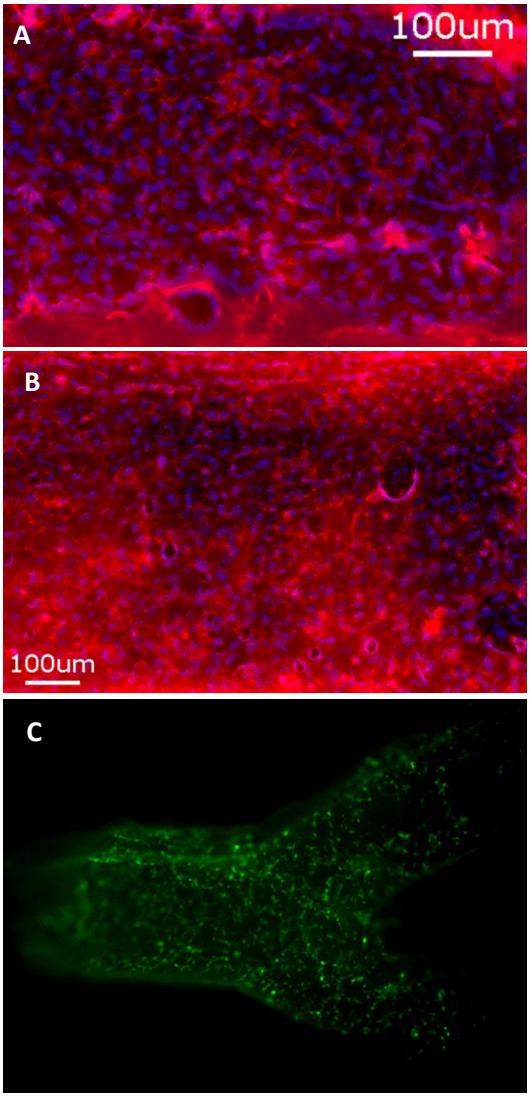

Figure 20. Confluent HUVEC layer formation on the channel walls after **a)** 3 and **b)** 7 days culture. DAPI (blue) was used to stain nucleus and VE-cadherin stain (red) represented junctions between endothelial cells. **c)** HUVECs (green) seeding on the branched channel walls after 3 days culture.

of silk [86]. According to previous study, the average pore size of the silk sponge can also be adjusted based on the freezing reagent including liquid nitrogen, dry ice with 99.8% ethanol or dry ice with 70% ethanol. The higher the freezing rate was, the larger the pore size achieved [64].

Through modifying the anisotropic structure, the silk-based construct is also able to achieve anisotropic diffusion of molecules with sizes similar to growth factors and proteins. Transportations of growth factors and proteins secreted from cells are important in inducing signal pathways, regulating metabolic activities and remodeling ECM environment [113, 114]. The diffusion coefficients measured in natural tissues varied significantly with different types of tissue and sizes of the diffusion molecules [106, 115, 116]. In heart muscle cells, 10 kDa dextran diffused at $(1.6 \pm 0.2)\times 10^{-7}$ cm^2/s in the transverse and $(1.9 \pm 0.3)\times 10^{-7}$ cm^2/s in the longitudinal directions [117]. For 3 kDa dextran, the measured anisotropic coefficients in the molecular layer of isolated turtle cerebellum were $(8.95 \pm 1.31)\times 10^{-7}$ cm^2/s and $(5.65 \pm 0.83)\times 10^{-7}$ cm^2/s at major and minor axis, respectively. And for 75kDa dextran, the measured anisotropic coefficients were $(1.24 \pm 0.11)\times 10^{-7}$ cm^2/s and $(0.7 \pm 0.09)\times 10^{-7}$ cm^2/s at major and minor axis, respectively. Although the diffusion coefficients in silk sponges are hard to match specific natural tissues, similar to the previous published results, the diffusion of dextran with larger molecular weight diffused slower than the dextran with smaller molecular weight. The values of measured diffusion coefficients might be much closer to the natural diffusion coefficients after growing cells in the silk scaffolds.

The microvascular system in the body, which is a complex branching network containing different sizes of blood vessels, supplies the surround tissues with sufficient oxygen and nutrients. To successfully build a complex engineering tissue construct *in vitro*, a similar branching network need to be built in the construct. Using the method in this project, the channels can be generated in the anisotropic

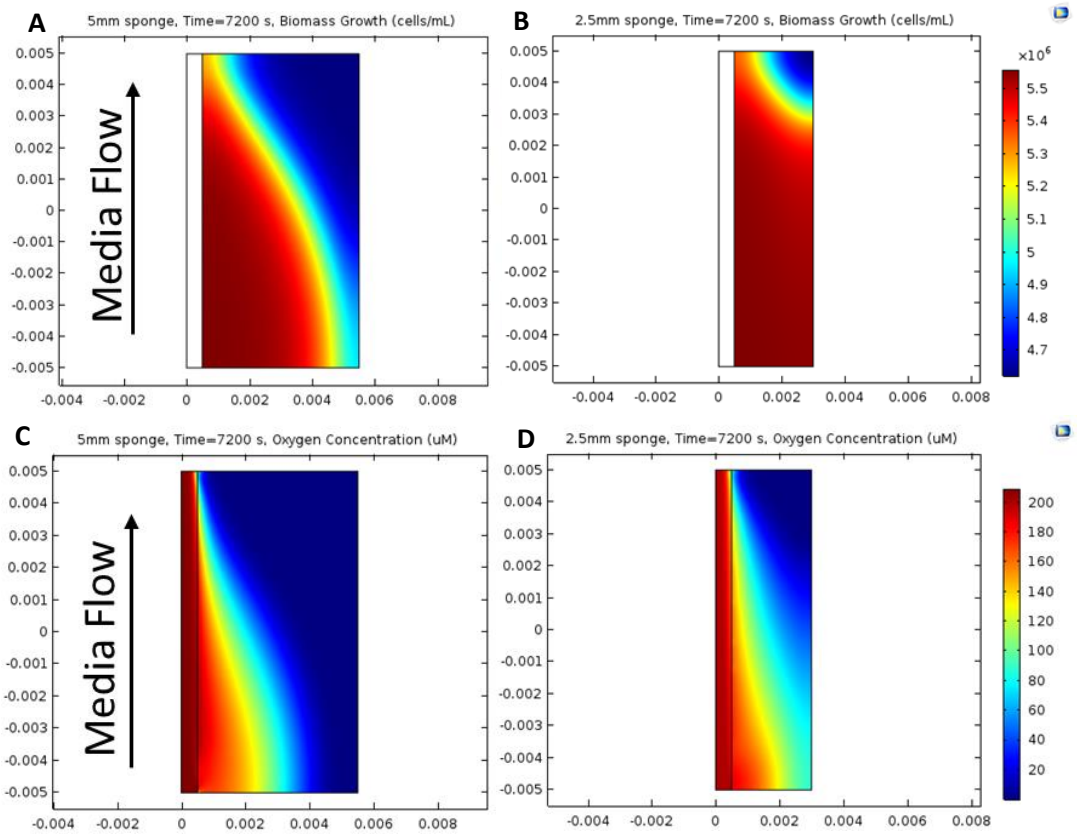

Figure 21. **a)** Simulation of biomass growth in the silk sponges with confluent HUVEC layer. **b)** Simulation of oxygen concentration in the silk sponges with confluent HUVEC layer.

silk scaffold with varied dimensions and shapes. Complex branching networks can be designed and generated by combining several layers of branched channels and thus mimic the morphologic characteristic of natural vascular system. Another advantage of this method is that the final dimension of the channels is half of the designed dimension, which resulted in easier generation of smaller channels.

The pore sizes on the silk film made channel walls could be adjusted from 10 μm to around 30 μm with PEG concentration varying from 1% to 10% [118]. The average size of endothelial cells is around 10 μm. Therefore, to determine the ability of the engineering silk-based construct in supporting vascularization, endothelial

cell adhesion, proliferation and the lumen formation were evaluated in the channels where silk films with no pores were used to make channel walls. The prevention of potential cell movement into surrounded sponge regions ensured HUVECs growing into confluency within 3 days of static culture. The maintenance of this confluent HUVECs layer was proved within 7 days.

If the channel walls were made using silk films with pore sizes larger than HUVCEs' diameter, the HUVECs would have the possibilities to move in to the bulk areas. This type of open channel configuration might be useful in investigating the fundamental mechanisms of endothelial lumen formation and capillary morphogenesis. Capillary morphogenesis has been found in collagen hydrogels with opened microchannels due to initiation of signaling pathways by native ECM cues [119]. Considering tissue engineering, capillary morphogenesis is necessary to provide sufficient oxygen and nutrients to the whole engineered construct. For investigating the capillary morphogenesis, bioreactors are under making to culture the silk-based constructs with fluid flow through channels for several months.

The model representing the silk constructs generated using COMSOL can be used to optimize the design of channel morphology and silk scaffold dimensions based on the oxygen concentration. With specific design, a hypoxia region can be generated to trigger the capillary formation. However, more information including the oxygen consumption of the cells in bulk space or the structure of branched channels need to be acquired to improve the COMSOL simulation.

This system can be used for further studies in development of regenerative tissue or long-term *in vitro* tissue models. HUVECs adhesion, proliferation and lumen formation were achieved in the channels which are the fundamentals of forming vascular system in the engineered construct. Co-culturing of other types of cells in the bulk space should be determined next to demonstrate the application of this system in various tissue formation with developed vascularization.

In conclusion, the project provides a new way to produce a critically sized engineered construct with anisotropic structures and branching networks. The silk-based scaffold can be tuned to achieve different microstructures and mechanical properties and thus successfully recapitulate the structures and functions of natural tissue. The findings of specific mechanical or biochemical cues for guiding desired stem cell differentiation collected from silk-hydrogel system developed in Chapter 3 can be also integrated into the silk scaffolds, and thus induce regeneration of targeted tissue including heart, cartilage, bone or liver.

Chapter 5 – Conclusions and Future Directions

5.1 Conclusion

In order to improve the efficacy of tissue regeneration, tissue engineered constructs have gained much focus as a potential treatment which might overcome several limitations of transplantation, synthetic prosthesis and mechanical devices. Recapsulation of specific natural tissue morphology and mechanical properties are essential for generation of porous 3D scaffolds with proper functions. Cells should be seeded into the 3D scaffold to form complex tissue *in vitro*. Stem cells are one of major cell sources used to create tissue engineered constructs. Therefore, fully understanding how the mechanical and biochemical cues affects the stem cell fate is important for improving efficiency of tissue engineered constructs.

The thesis provides a biocompatible, tunable silk system to systematically investigate the effects of substrate stiffness and mechanical stimulation on hMSCs fate, which is a well-established stem cell therapy. The hydrogel fibers can achieve a wide range of stiffness from 50 kPa to 150 kPa by changing the silk or H_2O_2 concentration. The survival and growth of encapsulated hMSCs are also proved in the silk hydrogel system for over 3 weeks culture. The hMSCs in silk hydrogel fibers at 50 kPa and 150 kPa both tended to enter the pre-osteoblast/adipocytes state after 2 weeks in static culture. With 24 h, 1 Hz cyclic stretching, osteo-differentiation was enhanced, while adipo-differentiation was suppressed.

This thesis also presents a new method to generate an anisotropic silk-based scaffold with branching networks for vascularization. Stable endothelialization with HUVECs was confirmed in the channels. Silk fibers in the scaffold aligned

with a specific direction. Analysis of anisotropic coefficients showed higher coefficients along the fiber directions than the coefficients perpendicular to the fiber directions, which comfirmed the anisotropic functions due to the fiber alignments. The simulation in COMSOL not only provided information to optimize the design of channels dimensions, but also indicated potential of using this system to generate hypoxia region for studing neuoroangiogenesis. Specific mechanical cues discovered in the silk-hydrogel system for guiding desired hMSCs fate can be integrated into the silk-based scaffold to generate specfic tissue such as heart or cartilage from differentiation of seeded hMSCs.

5.2 Future Directions for Evaluating hMSCs Fate

Further analysis of hMSC differentiation can be applied though protein expression. Lineage specific antibodies will be used to stain the cells to study the protein expression: Myogenesis Differentiation Protein 1 (MyoD1) and desmin for myogenesis; Core Binding Factor α1 (CBFA1) and osteocalcin for osteogenesis; and phosphorylated and dephosphorylated Neurofilament Heavy chain (NFH), Neurofilament Light chain (NFL) for neurogenesis [10]. The proliferation of hMSCs can also be evaluated by Ki67 staining (Abcam, Cambridge, MA, USA).

Besides mechanical properties, all the transplanted stem cells are exposed to various biochemical signals including ECM proteins, growth factors and adhesion molecules. Different tissues usually contain specific ECM components [82, 83]. Basement membranes are full of laminins and type IV collagen, while most of the soft connective tissue contains type I and III collagen [84]. The ECM components are also very different at various developmental stages. A study comparing cardiac

ECM at fetal, neonatal and adult stages indicated that fibronectin and periostin decrease with increased ages, and fibrillin-2 is only found in fetal and neonatal cardiac ECM. Type I collagen kept increasing from younger to older stage, and type III collagen only occurred in adult cardiac ECM [120]. Several experiments have been done to compare the effects of different ECM composition on stem cell fate. For example, a study combining the geometric cues and chemical cues showed that the stem cells in fibronectin or laminin patterns prefer an adipogenesis fate while the stem cells on collagen matrix tended to neurogenesis regardless of geometry [121]. Human elastin based biomimetic coating was also shown to stimulate osteogenesis of MSCs [122]. These all suggests that different ECM composition plays specific roles in regulation of stem cell fate.

Although a wide range of studies have been done on investigating how mechanical or biochemical factors affect stem cell fate at some aspects, fewer experiments combine mechanical and biochemical factors in a system to investigate stem cell fate when both substrate stiffness and ECM components are changing. Therefore, the developed silk hydrogel-based system can be made with addition of specific biochemical cues to study synergistic effects on stem cell fate by mechanical and biochemical signals.

If the silk system can be further optimized to guide the differentiation of hMSCs *in vivo* based on the studies *in vitro*, more factors such as electrical stimulation can be also added to this system. Furthermore, a mathematical model can be developed to represent the relationship between factors and stem cell fate and predict the potential differentiation of hMSCs, which would improve the design of stem cell

therapies and thus contribute to improving tissue regeneration in clinical treatment. Once the methods for analyzing multi-factors induced hMSCs fate can be established, other cell types such as ihPSCs or progenitor cells can also be investigated using this method.

5.3 Future Directions for Silk Scaffold

Once the silk-based tissue engineered constructs have been established, different components could be added into the constructs to further optimize the functions and host-construct interface.

Establishing a functional interface between host tissue and engineered constructs remain challenges in post-implantation [123, 124]. Differences in biomechanical properties between host tissue and an implanted silk-based engineered construct would inhibit cell infiltration and host tissue integration. The formation of a barrier-like fibrous capsule also limits vascularization and host integration of the implanted scaffold [125]. Hydrogel-type coatings, such as poly(hydroxylethyl methacrylate) (PHEMA), PEG and poly(vinyl-alcohol) (PVA), have been applied to overcome the foreign body response and improve device/host tissue interactions of implantable devices [126]. However, the chemical agents and mismatched biochemical properties could cause several biocompatibility issues [127]. Because the complex biochemical environment of the ECM plays an important role in regulating cell adhesion, metabolism and gene expression [128]. ECM-based hydrogels might successfully recapitulate the native tissue biochemical microenvironment containing tissue specific cues, and thus improves host cell infiltration and tissue integration [129].

Several anti-inflammation therapies are found to reduce fibrous capsule formation such as tanshinone IIA (Tan IIA) [130, 131], dexamethasone (DEX) [132-134], methylprednisolone [135], and Prostaglandin E2 (PGE2). DEX is preferred in the proposed work because it is an FDA approved anti-inflammatory drug that has been widely used in minimizing host immune responses. However, the disadvantages of the DEX include their inhibition on vascularization, wound healing and tissue regeneration [132, 136]. Therefore, the silk-based engineered constructs can be coated with a micro scale layer of DEX-loaded ECM hydrogel to reduce the formation of a fibrous capsule immediately after implantation and also prevent the potential side effects in the long term.

Poor electrical conductivity is another major limitation of tissue regeneration in cardiac and neural tissue reported in the literature. Many conductive components including gold/silver nanowires [137], carbon nanotubes (CNTs) [138, 139], and conducting polymers have been investigated to improve electrical communication between cells in the tissue engineered constructs due to their superior electrical conductivity. Therefore, conductive components can be also incorporated into the silk-based engineered constructs in the applications of cardiac or neural tissue regeneration.

With application of further development on the project in this thesis, the silk-hydrogel system is hypothesized to systematically investigate physical and biochemical cues in differentiating stem cells into specific lineage. The information of differentiation cues is expected to integrate into the silk-based scaffold

developed in the project to optimize the scaffold design and thus leads to fully regeneration into desired tissue including heart, cartilage, bone and liver.

References

[1] F.J. O'brien, Biomaterials & scaffolds for tissue engineering, Materials today 14(3) (2011) 88-95.
[2] T.R. Cox, J.T. Erler, Remodeling and homeostasis of the extracellular matrix: implications for fibrotic diseases and cancer, Disease models & mechanisms 4(2) (2011) 165-178.
[3] E.C. Novosel, C. Kleinhans, P.J. Kluger, Vascularization is the key challenge in tissue engineering, Advanced drug delivery reviews 63(4-5) (2011) 300-311.
[4] M. Breitbach, T. Bostani, W. Roell, Y. Xia, O. Dewald, J.M. Nygren, J.W. Fries, K. Tiemann, H. Bohlen, J. Hescheler, Potential risks of bone marrow cell transplantation into infarcted hearts, Blood 110(4) (2007) 1362-1369.
[5] M. Rothdiener, M. Hegemann, T. Uynuk-Ool, B. Walters, P. Papugy, P. Nguyen, V. Claus, T. Seeger, U. Stoeckle, K.A. Boehme, Stretching human mesenchymal stromal cells on stiffness-customized collagen type I generates a smooth muscle marker profile without growth factor addition, Scientific reports 6 (2016) 35840.
[6] B.P. Partlow, C.W. Hanna, J. Rnjak-Kovacina, J.E. Moreau, M.B. Applegate, K.A. Burke, B. Marelli, A.N. Mitropoulos, F.G. Omenetto, D.L. Kaplan, Highly tunable elastomeric silk biomaterials, Advanced functional materials 24(29) (2014) 4615-4624.
[7] A.E. Kuriyan, T.A. Albini, J.H. Townsend, M. Rodriguez, H.K. Pandya, R.E. Leonard, M.B. Parrott, P.J. Rosenfeld, H.W. Flynn Jr, J.L. Goldberg, Vision loss after intravitreal injection of autologous "stem cells" for AMD, N Engl J Med 2017(376) (2017) 1047-1053.
[8] K.J.P. Adrian McArdle, Michael T. Chung, Michael S. Hu, Graham Walmsley, Andrew Zimmermann, Victor W. Wong, Brian Hsueh, Andrew S. Chung, Geoffrey C. Gurtner, H. Peter Lorenz, Michael T. Longaker and Derrick C. Wan, Manipulation of Stem Cells and their Micro environment for Tissue Engineering, Surgery Curr Res 3(134) (2013).
[9] S. Browne, A. Pandit, Biomaterial-mediated modification of the local inflammatory environment, Frontiers in bioengineering and biotechnology 3 (2015) 67.
[10] A.J. Engler, S. Sen, H.L. Sweeney, D.E. Discher, Matrix elasticity directs stem cell lineage specification, Cell 126(4) (2006) 677-689.
[11] C. Denning, V. Borgdorff, J. Crutchley, K.S. Firth, V. George, S. Kalra, A. Kondrashov, M.D. Hoang, D. Mosqueira, A. Patel, Cardiomyocytes from human pluripotent stem cells: From laboratory curiosity to industrial biomedical platform, Biochimica et Biophysica Acta (BBA)-Molecular Cell Research 1863(7) (2016) 1728-1748.
[12] D.M. Sosin, J.E. Sniezek, R.J. Waxweiler, Trends in death associated with traumatic brain injury, 1979 through 1992: success and failure, Jama 273(22) (1995) 1778-1780.
[13] S. Goldman, G. Johnson, J.N. Cohn, G. Cintron, R. Smith, G. Francis, Mechanism of death in heart failure. The Vasodilator-Heart Failure Trials. The V-HeFT VA Cooperative Studies Group, Circulation 87(6 Suppl) (1993) VI24-31.
[14] P.S. Kamath, R.H. Wiesner, M. Malinchoc, W. Kremers, T.M. Therneau, C.L. Kosberg, G. D'Amico, E.R. Dickson, W. Kim, A model to predict survival in patients with end-stage liver disease, Hepatology 33(2) (2001) 464-470.
[15] D. Lloyd-Jones, R. Adams, M. Carnethon, G. De Simone, T.B. Ferguson, K. Flegal, E. Ford, K. Furie, A. Go, K. Greenlund, Heart disease and stroke statistics-2009 update: a report from the American Heart Association Statistics Committee and Stroke Statistics Subcommittee, Circulation 119(3) (2009) e21-e181.
[16] B.-S. Kim, D.J. Mooney, Development of biocompatible synthetic extracellular matrices for tissue engineering, Trends in biotechnology 16(5) (1998) 224-230.

[17] J. Zhang, Engineered tissue patch for cardiac cell therapy, Current treatment options in cardiovascular medicine 17(8) (2015) 37.
[18] Q. Wang, H. Yang, A. Bai, W. Jiang, X. Li, X. Wang, Y. Mao, C. Lu, R. Qian, F. Guo, Functional engineered human cardiac patches prepared from nature's platform improve heart function after acute myocardial infarction, Biomaterials 105 (2016) 52-65.
[19] M. Radisic, K.L. Christman, Materials science and tissue engineering: repairing the heart, Mayo Clinic Proceedings, Elsevier, 2013, pp. 884-898.
[20] S.T. Kurhade, M. Momin, P. Khanekar, S. Mhatre, Novel biocompatible honey hydrogel wound healing sponge for chronic ulcers, International Journal of Drug Delivery 5(4) (2013) 353.
[21] T. Okamoto, Y. Yamamoto, M. Gotoh, C.-L. Huang, T. Nakamura, Y. Shimizu, Y. Tabata, H. Yokomise, Slow release of bone morphogenetic protein 2 from a gelatin sponge to promote regeneration of tracheal cartilage in a canine model, The Journal of thoracic and cardiovascular surgery 127(2) (2004) 329-334.
[22] W.J. Parks, T.D. Ngo, W.H. Plauth, E.R. Bank, S.K. Sheppard, R.I. Pettigrew, W.H. Williams, Incidence of aneurysm formation after Dacron patch aortoplasty repair for coarctation of the aorta: long-term results and assessment utilizing magnetic resonance angiography with three-dimensional surface rendering, Journal of the American College of Cardiology 26(1) (1995) 266-271.
[23] K.L. Fujimoto, J. Guan, H. Oshima, T. Sakai, W.R. Wagner, In vivo evaluation of a porous, elastic, biodegradable patch for reconstructive cardiac procedures, The Annals of thoracic surgery 83(2) (2007) 648-654.
[24] J.M. Wainwright, R. Hashizume, K.L. Fujimoto, N.T. Remlinger, C. Pesyna, W.R. Wagner, K. Tobita, T.W. Gilbert, S.F. Badylak, Right ventricular outflow tract repair with a cardiac biologic scaffold, Cells Tissues Organs 195(1-2) (2012) 159-170.
[25] J. Yang, J. Bei, S. Wang, Enhanced cell affinity of poly (D, L-lactide) by combining plasma treatment with collagen anchorage, Biomaterials 23(12) (2002) 2607-2614.
[26] C.R. Nuttelman, D.J. Mortisen, S.M. Henry, K.S. Anseth, Attachment of fibronectin to poly (vinyl alcohol) hydrogels promotes NIH3T3 cell adhesion, proliferation, and migration, Journal of Biomedical Materials Research Part A 57(2) (2001) 217-223.
[27] D.B. Kolesky, R.L. Truby, A. Gladman, T.A. Busbee, K.A. Homan, J.A. Lewis, 3D bioprinting of vascularized, heterogeneous cell-laden tissue constructs, Advanced materials 26(19) (2014) 3124-3130.
[28] M.D. Tang, A.P. Golden, J. Tien, Fabrication of Collagen Gels That Contain Patterned, Micrometer-Scale Cavities, Advanced materials 16(15) (2004) 1345-1348.
[29] I. Vollert, M. Seiffert, J. Bachmair, M. Sander, A. Eder, L. Conradi, A. Vogelsang, T. Schulze, J. Uebeler, W. Holnthoner, In vitro perfusion of engineered heart tissue through endothelialized channels, Tissue engineering Part A 20(3-4) (2013) 854-863.
[30] B. Zhang, M. Montgomery, M.D. Chamberlain, S. Ogawa, A. Korolj, A. Pahnke, L.A. Wells, S.p. Massé, J. Kim, L. Reis, Biodegradable scaffold with built-in vasculature for organ-on-a-chip engineering and direct surgical anastomosis, Nature materials 15(6) (2016) 669.
[31] Z. Li, J. Guan, Hydrogels for cardiac tissue engineering, Polymers 3(2) (2011) 740-761.
[32] G. Vunjak-Novakovic, N. Tandon, A. Godier, R. Maidhof, A. Marsano, T.P. Martens, M. Radisic, Challenges in cardiac tissue engineering, Tissue Engineering Part B: Reviews 16(2) (2009) 169-187.
[33] V.F. Segers, R.T. Lee, Stem-cell therapy for cardiac disease, Nature 451(7181) (2008) 937-942.

[34] Y. Zhu, X. Chen, X. Yang, J. Ji, A.H. Hashash, Stem Cells in Lung Repair and Regeneration: Current Applications and Future Promise, Journal of cellular physiology (2017).
[35] J. Ankrum, J.M. Karp, Mesenchymal stem cell therapy: two steps forward, one step back, Trends in molecular medicine 16(5) (2010) 203-209.
[36] B. Huang, X. Cheng, H. Wang, W. Huang, D. Wang, K. Zhang, H. Zhang, Z. Xue, Y. Da, N. Zhang, Mesenchymal stem cells and their secreted molecules predominantly ameliorate fulminant hepatic failure and chronic liver fibrosis in mice respectively, Journal of translational medicine 14(1) (2016) 45.
[37] Z. Liu, F. Meng, C. Li, X. Zhou, X. Zeng, Y. He, R.J. Mrsny, M. Liu, X. Hu, J.-F. Hu, Human umbilical cord mesenchymal stromal cells rescue mice from acetaminophen-induced acute liver failure, Cytotherapy 16(9) (2014) 1207-1219.
[38] J.M. Hare, J.E. Fishman, G. Gerstenblith, D.L.D. Velazquez, J.P. Zambrano, V.Y. Suncion, M. Tracy, E. Ghersin, P.V. Johnston, J.A. Brinker, Comparison of allogeneic vs autologous bone marrow-derived mesenchymal stem cells delivered by transendocardial injection in patients with ischemic cardiomyopathy: the POSEIDON randomized trial, Jama 308(22) (2012) 2369-2379.
[39] Y. Wang, U.-J. Kim, D.J. Blasioli, H.-J. Kim, D.L. Kaplan, In vitro cartilage tissue engineering with 3D porous aqueous-derived silk scaffolds and mesenchymal stem cells, Biomaterials 26(34) (2005) 7082-7094.
[40] J.R. Mauney, T. Nguyen, K. Gillen, C. Kirker-Head, J.M. Gimble, D.L. Kaplan, Engineering adipose-like tissue in vitro and in vivo utilizing human bone marrow and adipose-derived mesenchymal stem cells with silk fibroin 3D scaffolds, Biomaterials 28(35) (2007) 5280-5290.
[41] V. Volarevic, B.S. Markovic, M. Gazdic, A. Volarevic, N. Jovicic, N. Arsenijevic, L. Armstrong, V. Djonov, M. Lako, M. Stojkovic, Ethical and Safety Issues of Stem Cell-Based Therapy, Int J Med Sci 15(1) (2018) 36-45.
[42] L. Macri-Pellizzeri, E.M. De-Juan-Pardo, F. Prosper, B. Pelacho, Role of substrate biomechanics in controlling (stem) cell fate: implications in regenerative medicine, Journal of tissue engineering and regenerative medicine (2017).
[43] K.M. Adlerz, H. Aranda-Espinoza, H.N. Hayenga, Substrate elasticity regulates the behavior of human monocyte-derived macrophages, European Biophysics Journal 45(4) (2016) 301-309.
[44] M. Prager-Khoutorsky, A. Lichtenstein, R. Krishnan, K. Rajendran, A. Mayo, Z. Kam, B. Geiger, A.D. Bershadsky, Fibroblast polarization is a matrix-rigidity-dependent process controlled by focal adhesion mechanosensing, Nature cell biology 13(12) (2011) 1457-1465.
[45] M. Maldonado, G. Ico, K. Low, R.J. Luu, J. Nam, Enhanced Lineage-Specific Differentiation Efficiency of Human Induced Pluripotent Stem Cells by Engineering Colony Dimensionality Using Electrospun Scaffolds, Advanced healthcare materials 5(12) (2016) 1408-1412.
[46] M. Maldonado, R.J. Luu, G. Ico, A. Ospina, D. Myung, H.P. Shih, J. Nam, Lineage-and developmental stage-specific mechanomodulation of induced pluripotent stem cell differentiation, Stem cell research & therapy 8(1) (2017) 216.
[47] H.Y. Nam, H.R.B. Raghavendran, B. Pingguan-Murphy, A.A. Abbas, A.M. Merican, T. Kamarul, Fate of tenogenic differentiation potential of human bone marrow stromal cells by uniaxial stretching affected by stretch-activated calcium channel agonist gadolinium, Plos One 12(6) (2017) e0178117.

[48] T. Uynuk-Ool, M. Rothdiener, B. Walters, M. Hegemann, J. Palm, P. Nguyen, T. Seeger, U. Stöckle, J.P. Stegemann, W.K. Aicher, The geometrical shape of mesenchymal stromal cells measured by quantitative shape descriptors is determined by the stiffness of the biomaterial and by cyclic tensile forces, Journal of Tissue Engineering and Regenerative Medicine (2017).
[49] W. Grier, A. Moy, B. Harley, Cyclic tensile strain enhances human mesenchymal stem cell Smad 2/3 activation and tenogenic differentiation in anisotropic collagen-glycosaminoglycan scaffolds, European cells & materials 33 (2017) 227-239.
[50] Y. Qiu, J. Lei, T.J. Koob, J.S. Temenoff, Cyclic tension promotes fibroblastic differentiation of human MSCs cultured on collagen-fibre scaffolds, Journal of tissue engineering and regenerative medicine 10(12) (2016) 989-999.
[51] J.S. Lee, L. Ha, J.-H. Park, J.Y. Lim, Mechanical stretch suppresses BMP4 induction of stem cell adipogenesis via upregulating ERK but not through downregulating Smad or p38, Biochemical and biophysical research communications 418(2) (2012) 278-283.
[52] Y. Song, Y. Tang, J. Song, M. Lei, P. Liang, T. Fu, X. Su, P. Zhou, L. Yang, E. Huang, Cyclic mechanical stretch enhances BMP9-induced osteogenic differentiation of mesenchymal stem cells, International orthopaedics (2018) 1-9.
[53] L. Sun, L. Qu, R. Zhu, H. Li, Y. Xue, X. Liu, J. Fan, H. Fan, Effects of Mechanical Stretch on Cell Proliferation and Matrix Formation of Mesenchymal Stem Cell and Anterior Cruciate Ligament Fibroblast, Stem cells international 2016 (2016).
[54] B. Walters, T. Uynuk-Ool, M. Rothdiener, J. Palm, M.L. Hart, J.P. Stegemann, B. Rolauffs, Engineering the geometrical shape of mesenchymal stromal cells through defined cyclic stretch regimens, Scientific reports 7(1) (2017) 6640.
[55] Y. Yang, S. Beqaj, P. Kemp, I. Ariel, L. Schuger, Stretch-induced alternative splicing of serum response factor promotes bronchial myogenesis and is defective in lung hypoplasia, The Journal of clinical investigation 106(11) (2000) 1321-1330.
[56] C. Vepari, D.L. Kaplan, Silk as a biomaterial, Progress in polymer science 32(8) (2007) 991-1007.
[57] R.L. Horan, K. Antle, A.L. Collette, Y. Wang, J. Huang, J.E. Moreau, V. Volloch, D.L. Kaplan, G.H. Altman, In vitro degradation of silk fibroin, Biomaterials 26(17) (2005) 3385-3393.
[58] Y. Yang, X. Chen, F. Ding, P. Zhang, J. Liu, X. Gu, Biocompatibility evaluation of silk fibroin with peripheral nerve tissues and cells in vitro, Biomaterials 28(9) (2007) 1643-1652.
[59] L. Meinel, S. Hofmann, V. Karageorgiou, C. Kirker-Head, J. McCool, G. Gronowicz, L. Zichner, R. Langer, G. Vunjak-Novakovic, D.L. Kaplan, The inflammatory responses to silk films in vitro and in vivo, Biomaterials 26(2) (2005) 147-155.
[60] D.N. Rockwood, R.C. Preda, T. Yücel, X. Wang, M.L. Lovett, D.L. Kaplan, Materials fabrication from Bombyx mori silk fibroin, Nature protocols 6(10) (2011) 1612-1631.
[61] W.L. Stoppel, D. Hu, I.J. Domian, D.L. Kaplan, L.D. Black III, Anisotropic silk biomaterials containing cardiac extracellular matrix for cardiac tissue engineering, Biomedical materials 10(3) (2015) 034105.
[62] M.C.T. Asuncion, J.C.-H. Goh, S.-L. Toh, Anisotropic silk fibroin/gelatin scaffolds from unidirectional freezing, Materials Science and Engineering: C 67 (2016) 646-656.
[63] Y. Sang, M. Li, J. Liu, Y. Yao, Z. Ding, L. Wang, L. Xiao, Q. Lu, X. Fu, D.L. Kaplan, Biomimetic Silk Scaffolds with an Amorphous Structure for Soft Tissue Engineering, ACS applied materials & interfaces (2018).

[64] L.S. Wray, J. Rnjak-Kovacina, B.B. Mandal, D.F. Schmidt, E.S. Gil, D.L. Kaplan, A silk-based scaffold platform with tunable architecture for engineering critically-sized tissue constructs, Biomaterials 33(36) (2012) 9214-9224.
[65] X. Wang, J.A. Kluge, G.G. Leisk, D.L. Kaplan, Sonication-induced gelation of silk fibroin for cell encapsulation, Biomaterials 29(8) (2008) 1054-1064.
[66] T. Yucel, P. Cebe, D.L. Kaplan, Vortex-induced injectable silk fibroin hydrogels, Biophysical journal 97(7) (2009) 2044-2050.
[67] B.P. Partlow, C.W. Hanna, J. Rnjak-Kovacina, J.E. Moreau, M.B. Applegate, K.A. Burke, B. Marelli, A.N. Mitropoulos, F.G. Omenetto, D.L. Kaplan, Highly tunable elastomeric silk biomaterials, Adv Funct Mater 24(29) (2014) 4615-4624.
[68] S.A. Bradner, B.P. Partlow, P. Cebe, F.G. Omenetto, D.L. Kaplan, Fabrication of Elastomeric Silk Fibers, Biopolymers.
[69] G.J. Her, H.-C. Wu, M.-H. Chen, M.-Y. Chen, S.-C. Chang, T.-W. Wang, Control of three-dimensional substrate stiffness to manipulate mesenchymal stem cell fate toward neuronal or glial lineages, Acta Biomaterialia 9(2) (2013) 5170-5180.
[70] D.E. Discher, D.J. Mooney, P.W. Zandstra, Growth factors, matrices, and forces combine and control stem cells, Science 324(5935) (2009) 1673-1677.
[71] A.W. James, Review of signaling pathways governing MSC osteogenic and adipogenic differentiation, Scientifica 2013 (2013).
[72] L.C. Amado, A.P. Saliaris, K.H. Schuleri, M.S. John, J.-S. Xie, S. Cattaneo, D.J. Durand, T. Fitton, J.Q. Kuang, G. Stewart, Cardiac repair with intramyocardial injection of allogeneic mesenchymal stem cells after myocardial infarction, Proceedings of the National Academy of Sciences of the United States of America 102(32) (2005) 11474-11479.
[73] M. Alfaifi, Y.W. Eom, P.N. Newsome, S.K. Baik, Mesenchymal stromal cell therapy for liver diseases, Journal of hepatology (2018).
[74] A. Bartczak, I. McGilvray, A. Keating, Mesenchymal stromal cell therapy to promote cardiac tissue regeneration and repair, Current opinion in organ transplantation 22(1) (2017) 86-96.
[75] M.F. Pittenger, A.M. Mackay, S.C. Beck, R.K. Jaiswal, R. Douglas, J.D. Mosca, M.A. Moorman, D.W. Simonetti, S. Craig, D.R. Marshak, Multilineage potential of adult human mesenchymal stem cells, science 284(5411) (1999) 143-147.
[76] Z.J. Liu, Y. Zhuge, O.C. Velazquez, Trafficking and differentiation of mesenchymal stem cells, Journal of cellular biochemistry 106(6) (2009) 984-991.
[77] J.-W. Lee, S.-H. Lee, Y.-J. Youn, M.-S. Ahn, J.-Y. Kim, B.-S. Yoo, J. Yoon, W. Kwon, I.-S. Hong, K. Lee, A randomized, open-label, multicenter trial for the safety and efficacy of adult mesenchymal stem cells after acute myocardial infarction, Journal of Korean medical science 29(1) (2014) 23-31.
[78] D.E. Atsma, W.E. Fibbe, T.J. Rabelink, Opportunities and challenges for mesenchymal stem cell-mediated heart repair, Current opinion in lipidology 18(6) (2007) 645-649.
[79] V. Volarevic, N. Arsenijevic, M.L. Lukic, M. Stojkovic, Concise review: mesenchymal stem cell treatment of the complications of diabetes mellitus, Stem cells 29(1) (2011) 5-10.
[80] J.K. Leach, J. Whitehead, Materials-directed differentiation of mesenchymal stem cells for tissue engineering and regeneration, ACS Biomaterials Science & Engineering (2017).
[81] A. Higuchi, Q.-D. Ling, Y. Chang, S.-T. Hsu, A. Umezawa, Physical cues of biomaterials guide stem cell differentiation fate, Chemical reviews 113(5) (2013) 3297-3328.

[82] C. Frantz, K.M. Stewart, V.M. Weaver, The extracellular matrix at a glance, J Cell Sci 123(24) (2010) 4195-4200.
[83] V.Z. Beachley, M.T. Wolf, K. Sadtler, S.S. Manda, H. Jacobs, M.R. Blatchley, J.S. Bader, A. Pandey, D. Pardoll, J.H. Elisseeff, Tissue matrix arrays for high-throughput screening and systems analysis of cell function, Nature methods 12(12) (2015) 1197-1204.
[84] F.M. Watt, W.T. Huck, Role of the extracellular matrix in regulating stem cell fate, Nature reviews Molecular cell biology 14(8) (2013) 467-473.
[85] R. Li, L. Liang, Y. Dou, Z. Huang, H. Mo, Y. Wang, B. Yu, Mechanical stretch inhibits mesenchymal stem cell adipogenic differentiation through TGF-1/Smad2 signaling, Journal of biomechanics 48(13) (2015) 3665-3671.
[86] J.E. Brown, J.E. Moreau, A.M. Berman, H.J. McSherry, J.M. Coburn, D.F. Schmidt, D.L. Kaplan, Shape Memory Silk Protein Sponges for Minimally Invasive Tissue Regeneration, Advanced healthcare materials 6(2) (2017).
[87] Y. Cai, J. Guo, C. Chen, C. Yao, S.-M. Chung, J. Yao, I.-S. Lee, X. Kong, Silk fibroin membrane used for guided bone tissue regeneration, Materials Science and Engineering: C 70 (2017) 148-154.
[88] L.P. Yan, J.M. Oliveira, A.L. Oliveira, R.L. Reis, Core-shell silk hydrogels with spatially tuned conformations as drug-delivery system, Journal of tissue engineering and regenerative medicine 11(11) (2017) 3168-3177.
[89] B. Crivelli, S. Perteghella, E. Bari, M. Sorrenti, G. Tripodo, T. Chlapanidas, M.L. Torre, Silk nanoparticles: from inert supports to bioactive natural carriers for drug delivery, Soft matter (2018).
[90] D.L. Kaplan, T. Yucel, M.L. Lovett, X. Wang, Silk reservoirs for drug delivery, Google Patents, 2017.
[91] M. McGill, J.M. Coburn, B.P. Partlow, X. Mu, D.L. Kaplan, Molecular and macro-scale analysis of enzyme-crosslinked silk hydrogels for rational biomaterial design, Acta biomaterialia 63 (2017) 76-84.
[92] J.N. Rodríguez-López, D.J. Lowe, J. Hernández-Ruiz, A.N. Hiner, F. García-Cánovas, R.N. Thorneley, Mechanism of reaction of hydrogen peroxide with horseradish peroxidase: identification of intermediates in the catalytic cycle, Journal of the American Chemical Society 123(48) (2001) 11838-11847.
[93] N.R. Raia, B.P. Partlow, M. McGill, E.P. Kimmerling, C.E. Ghezzi, D.L. Kaplan, Enzymatically crosslinked silk-hyaluronic acid hydrogels, Biomaterials 131 (2017) 58-67.
[94] W.L. Stoppel, A.E. Gao, A.M. Greaney, B.P. Partlow, R.C. Bretherton, D.L. Kaplan, L.D. Black, Elastic, silk-cardiac extracellular matrix hydrogels exhibit time-dependent stiffening that modulates cardiac fibroblast response, Journal of Biomedical Materials Research Part A 104(12) (2016) 3058-3072.
[95] N. Huebsch, P.R. Arany, A.S. Mao, D. Shvartsman, O.A. Ali, S.A. Bencherif, J. Rivera-Feliciano, D.J. Mooney, Harnessing traction-mediated manipulation of the cell/matrix interface to control stem-cell fate, Nature materials 9(6) (2010) 518.
[96] X.D. Chen, H.Y. Qian, L. Neff, K. Satomura, M.C. Horowitz, Thy-1 Antigen Expression by Cells in the Osteoblast Lineage, Journal of Bone and Mineral Research 14(3) (1999) 362-375.
[97] M.T. Chung, C. Liu, J.S. Hyun, D.D. Lo, D.T. Montoro, M. Hasegawa, S. Li, M. Sorkin, R. Rennert, M. Keeney, CD90 (Thy-1)-positive selection enhances osteogenic capacity of human adipose-derived stromal cells, Tissue Engineering Part A 19(7-8) (2013) 989-997.
[98] B. Lecka-Czernik, L.J. Suva, Resolving the two "bony" faces of PPAR γ , PPAR research 2006 (2006).

[99] Y. Tang, S.J. Weiss, Snail/Slug-YAP/TAZ complexes cooperatively regulate mesenchymal stem cell function and bone formation, Cell Cycle 16(5) (2017) 399-405.
[100] T. Stylianopoulos, B. Diop-Frimpong, L.L. Munn, R.K. Jain, Diffusion anisotropy in collagen gels and tumors: the effect of fiber network orientation, Biophysical journal 99(10) (2010) 3119-3128.
[101] M.S. Spach, J.F. Heidlage, P.C. Dolber, C. Roger, Changes in anisotropic conduction caused by remodeling cell size and the cellular distribution of gap junctions and Na+ channels, Journal of electrocardiology 34(4) (2001) 69-76.
[102] J.E. Saffitz, H.L. Kanter, K.G. Green, T.K. Tolley, E.C. Beyer, Tissue-specific determinants of anisotropic conduction velocity in canine atrial and ventricular myocardium, Circulation research 74(6) (1994) 1065-1070.
[103] I.-H. Jo, K.-H. Shin, Y.-M. Soon, Y.-H. Koh, J.-H. Lee, H.-E. Kim, Highly porous hydroxyapatite scaffolds with elongated pores using stretched polymeric sponges as novel template, Materials Letters 63(20) (2009) 1702-1704.
[104] L.M. Mathieu, T.L. Mueller, P.-E. Bourban, D.P. Pioletti, R. Müller, J.-A.E. Månson, Architecture and properties of anisotropic polymer composite scaffolds for bone tissue engineering, Biomaterials 27(6) (2006) 905-916.
[105] N. Davidenko, T. Gibb, C. Schuster, S.M. Best, J.J. Campbell, C.J. Watson, R.E. Cameron, Biomimetic collagen scaffolds with anisotropic pore architecture, Acta biomaterialia 8(2) (2012) 667-676.
[106] F. Xiao, C. Nicholson, J. Hrabe, S. Hrabetova, Diffusion of flexible random-coil dextran polymers measured in anisotropic brain extracellular space by integrative optical imaging, Biophys J 95(3) (2008) 1382-92.
[107] H. Ye, D.B. Das, J.T. Triffitt, Z. Cui, Modelling nutrient transport in hollow fibre membrane bioreactors for growing three-dimensional bone tissue, Journal of Membrane Science 272(1-2) (2006) 169-178.
[108] M. Shakeel, P.C. Matthews, R.S. Graham, S.L. Waters, A continuum model of cell proliferation and nutrient transport in a perfusion bioreactor, Mathematical medicine and biology: a journal of the IMA 30(1) (2013) 21-44.
[109] M.L. Shuler, F. Kargi, M. DeLisa, Bioprocess engineering: basic concepts, Prentice Hall Englewood Cliffs, NJ2017.
[110] D.D. Streeter, D.L. Bassett, An engineering analysis of myocardial fiber orientation in pig's left ventricle in systole, The Anatomical Record 155(4) (1966) 503-511.
[111] I.J. LeGrice, B. Smaill, L. Chai, S. Edgar, J. Gavin, P.J. Hunter, Laminar structure of the heart: ventricular myocyte arrangement and connective tissue architecture in the dog, American Journal of Physiology-Heart and Circulatory Physiology 269(2) (1995) H571-H582.
[112] D.A. Cameron, The ultrastructure of bone, The biochemistry and physiology of bone 1 (2012) 191-236.
[113] D.M. Ignar-Trowbridge, K.G. Nelson, M.C. Bidwell, S.W. Curtis, T.F. Washburn, J.A. McLachlan, K.S. Korach, Coupling of dual signaling pathways: epidermal growth factor action involves the estrogen receptor, Proceedings of the National Academy of Sciences 89(10) (1992) 4658-4662.
[114] W.J. Fantl, J.A. Escobedo, G.A. Martin, C.W. Turck, M. del Rosario, F. McCormick, L.T. Williams, Distinct phosphotyrosines on a growth factor receptor bind to specific molecules that mediate different signaling pathways, Cell 69(3) (1992) 413-423.

[115] M.C. Papadopoulos, J.K. Kim, A.S. Verkman, Extracellular space diffusion in central nervous system: anisotropic diffusion measured by elliptical surface photobleaching, Biophys J 89(5) (2005) 3660-8.
[116] H.A. Leddy, F. Guilak, Site-specific molecular diffusion in articular cartilage measured using fluorescence recovery after photobleaching, Annals of biomedical engineering 31(7) (2003) 753-760.
[117] A. Illaste, M. Laasmaa, P. Peterson, M. Vendelin, Analysis of molecular movement reveals latticelike obstructions to diffusion in heart muscle cells, Biophysical Journal 102(4) (2012) 739-748.
[118] M. Lovett, C. Cannizzaro, L. Daheron, B. Messmer, G. Vunjak-Novakovic, D.L. Kaplan, Silk fibroin microtubes for blood vessel engineering, Biomaterials 28(35) (2007) 5271-5279.
[119] W. Koh, R.D. Mahan, G.E. Davis, Cdc42-and Rac1-mediated endothelial lumen formation requires Pak2, Pak4 and Par3, and PKC-dependent signaling, Journal of cell science 121(7) (2008) 989-1001.
[120] C. Williams, K.P. Quinn, I. Georgakoudi, L.D. Black III, Young developmental age cardiac extracellular matrix promotes the expansion of neonatal cardiomyocytes in vitro, Acta biomaterialia 10(1) (2014) 194-204.
[121] J. Lee, A.A. Abdeen, D. Zhang, K.A. Kilian, Directing stem cell fate on hydrogel substrates by controlling cell geometry, matrix mechanics and adhesion ligand composition, Biomaterials 34(33) (2013) 8140-8148.
[122] B.l. çelebi, M. Cloutier, R. Balloni, D. Mantovani, A. Bandiera, Human Elastin-Based Recombinant Biopolymers Improve Mesenchymal Stem Cell Differentiation, Macromolecular bioscience 12(11) (2012) 1546-1554.
[123] B.M. Ogle, N. Bursac, I. Domian, N.F. Huang, P. Menaschᅩ, C.E. Murry, B. Pruitt, M. Radisic, J.C. Wu, S.M. Wu, Distilling complexity to advance cardiac tissue engineering, Science translational medicine 8(342) (2016) 342ps13-342ps13.
[124] J.S. Wendel, L. Ye, P. Zhang, R.T. Tranquillo, J.J. Zhang, Functional consequences of a tissue-engineered myocardial patch for cardiac repair in a rat infarct model, Tissue Engineering Part A 20(7-8) (2014) 1325-1335.
[125] Y. Lee, J. Kwon, G. Khang, D. Lee, Reduction of inflammatory responses and enhancement of extracellular matrix formation by vanillin-incorporated poly (lactic-co-glycolic acid) scaffolds, Tissue Engineering Part A 18(19-20) (2012) 1967-1978.
[126] J.M. Morais, F. Papadimitrakopoulos, D.J. Burgess, Biomaterials/tissue interactions: possible solutions to overcome foreign body response, The AAPS journal 12(2) (2010) 188-196.
[127] T. Kamarul, G. Krishnamurithy, N.D. Salih, N.S. Ibrahim, H.R.B. Raghavendran, A.R. Suhaeb, D. Choon, Biocompatibility and toxicity of poly (vinyl alcohol)/N, O-carboxymethyl chitosan scaffold, The Scientific World Journal 2014 (2014).
[128] F. Gattazzo, A. Urciuolo, P. Bonaldo, Extracellular matrix: a dynamic microenvironment for stem cell niche, Biochimica et Biophysica Acta (BBA)-General Subjects 1840(8) (2014) 2506-2519.
[129] A. Hasan, A. Khattab, M.A. Islam, K.A. Hweij, J. Zeitouny, R. Waters, M. Sayegh, M.M. Hossain, A. Paul, Injectable hydrogels for cardiac tissue repair after myocardial infarction, Advanced Science 2(11) (2015).
[130] S. Gao, Z. Liu, H. Li, P.J. Little, P. Liu, S. Xu, Cardiovascular actions and therapeutic potential of tanshinone IIA, Atherosclerosis 220(1) (2012) 3-10.

[131] Q. Yu, L. Sheng, M. Yang, M. Zhu, X. Huang, Q. Li, Tanshinon IIA injection accelerates tissue expansion by reducing the formation of the fibrous capsule, Plos One 9(8) (2014) e105756.
[132] S.D. Patil, F. Papadmitrakopoulos, D.J. Burgess, Concurrent delivery of dexamethasone and VEGF for localized inflammation control and angiogenesis, Journal of controlled release 117(1) (2007) 68-79.
[133] M.J. Webber, J.B. Matson, V.K. Tamboli, S.I. Stupp, Controlled release of dexamethasone from peptide nanofiber gels to modulate inflammatory response, Biomaterials 33(28) (2012) 6823-6832.
[134] N. Bulow, E. Colpo, R. Pereira, E. Correa, E. Waczuk, M. Duarte, J. Rocha, Dexmedetomidine decreases the inflammatory response to myocardial surgery under mini-cardiopulmonary bypass, Brazilian Journal of Medical and Biological Research 49(4) (2016).
[135] J. Keski-Nisula, E. Pesonen, K.T. Olkkola, K. Peltola, P.J. Neuvonen, N. Tuominen, H. Sairanen, S. Andersson, P.K. Suominen, Methylprednisolone in neonatal cardiac surgery: reduced inflammation without improved clinical outcome, The Annals of thoracic surgery 95(6) (2013) 2126-2132.
[136] P.T. Thevenot, A.M. Nair, J. Shen, P. Lotfi, C.-Y. Ko, L. Tang, The effect of incorporation of SDF-1 α into PLGA scaffolds on stem cell recruitment and the inflammatory response, Biomaterials 31(14) (2010) 3997-4008.
[137] A. Wickham, M. Vagin, H. Khalaf, S. Bertazzo, P. Hodder, S. Dånmark, T.r. Bengtsson, J. Altimiras, D. Aili, Electroactive biomimetic collagen-silver nanowire composite scaffolds, Nanoscale 8(29) (2016) 14146-14155.
[138] H. Sun, J. Zhou, Z. Huang, L. Qu, N. Lin, C. Liang, R. Dai, L. Tang, F. Tian, Carbon nanotube-incorporated collagen hydrogels improve cell alignment and the performance of cardiac constructs, International journal of nanomedicine 12 (2017) 3109.
[139] E.L. Hopley, S. Salmasi, D.M. Kalaskar, A.M. Seifalian, Carbon nanotubes leading the way forward in new generation 3D tissue engineering, Biotechnology advances 32(5) (2014) 1000-1014.